Hydrogeological assessment of a deep-seated coastal landslide based on a multi-disciplinary approach

Guillaume Thirard, Gilles Grandjean, Yannick Thiery, Olivier Maquaire, Benjamin François, Candide Lissak, Stéphane Costa

Hydrogeological assessment of a deep-seated coastal landslide based on a multi-disciplinary approach

Guillaume Thirard[*1,2], *Gilles Grandjean*[2], *Yannick Thiery*[2], *Olivier Maquaire*[1], *Benjamin François*[2], *Candide Lissak*[1], *Stéphane Costa*[1]

[1]NORMANDIE UNIV, UNICAEN, CNRS, LETG, 14000 CAEN, France

[2]Bureau de Recherches Géologiques et Minières (BRGM), 3 avenue Claude Guillemin - BP 36009 - 45060 Orléans Cedex 2, France

***Contact: guillaume.thirard@unicaen.fr**

***Full postal address**: Laboratoire LETG-Caen Geophen, Université de Caen Normandie, Campus 1, Bâtiment A, Rez-de-jardin, ACS 65 - Esplanade de la paix, 14032 CAEN cedex 5 (France)

1. Introduction

Over the last decades, the joint use of multi-disciplinary investigation methods has been widely disseminated in the study of landslide behaviour (Caris and Van Asch, 1991; Jomard et al., 2007; Fressard et al., 2016; Denchik et al., 2019; Di Maio et al., 2020). It is known that no single method, whether direct or indirect, is able to reliably image the structure and dynamics affecting an unstable slope. A wide range of methods are available for researchers or practitioners to achieve this purpose, such as borehole descriptions, laboratory tests, geophysical surveys, and remote sensing techniques (Jongmans and Garambois, 2007; Chambers et al., 2011; Perrone et al., 2014). For hydrologically controlled landslides, a major issue is also the characterization of the water circulation, often affected by spatial and temporal variability, beyond the sole structural aspect (Malet et al., 2005).

Geophysical surveys are classically used for this type of study. The most common methods are seismic refraction and reflection, geoelectrical methods (electrical resistivity and self-potential), electromagnetic methods, and gravimetry. Each method has its own set of advantages and drawbacks (Frappa and Lebourg, 2001; Pazzi et al., 2019). Depending on the method, the use of geophysics allows the imaging of the subsurface from one to four dimensions (Jongmans and Garambois, 2007). These methods are most often used to study landslide structure, including lithostratigraphic alternation, bedrock depth, geological boundaries, and slip surfaces (Bogoslovsky and Ogilvy, 1977; Meric et al., 2005; Godio et al., 2006; Jomard et al., 2007; Göktürkler et al., 2008; Erginal et al., 2009; Schmutz et al., 2009; Chambers et al., 2011; Coulouma et al., 2012). Geophysics is also of real interest in determining the hydrogeological characteristics associated with a given structure (Grandjean et al., 2006; Jomard et al., 2007; Lee et al., 2008; Niesner and Weidinger, 2008; Chambers et al., 2011; Gance et al., 2016).

Geoelectrical methods are classically used for landslide studies (Grandjean et al., 2006; Jongmans and Garambois, 2007; Travelletti and Malet, 2012; Ekinci et al., 2013; Gance et al., 2016; Palis et al., 2017; Whiteley et al., 2019). Electrical resistivity tomography (ERT) is classified as an active method and is most often used in the form of two-dimensional profiles. It is designed to measure the electrical potential difference between two pairs of electrodes by injecting a direct current into the soil (Kearey et al., 2002; Whiteley et al., 2019). ERT can be used to assess the internal structure of landslides and highlight the moisture content of materials (Telford and Sheriff, 1990; Jongmans and Garambois, 2007; Shevnin et al., 2007; Chambers et al., 2011; Denchik et al., 2019; Pazzi et al., 2019). This method is particularly suitable to characterize the saturation of clay slides, which are very sensitive to the presence of water.

Self-potential (or spontaneous polarization) is a passive geoelectric method. This technique has been increasingly used in recent years in the field of hydrogeological studies and allows the characterization of the solid-liquid interface of porous media (Colangelo et al., 2006; Jardani et al., 2006; Roubinet et al., 2016; Cherubini, 2019) and highlighting of underground flows and drainage patterns (Revil et al., 1999; Chambers et al., 2011). This method is defined as the measurement of the electrical potential distribution at the soil surface without current injection (Naudet, 2004). SP measurements characterize a sum of potential electrical charges (superposition principle), including thermo-electric, electrochemical and electrokinetic mechanisms (Corwin and Hoover, 1979; Titov et al., 2002; Colangelo et al., 2006; Chambers et al., 2011). In the absence of telluric or chemical disturbances, the electrokinetic phenomenon (or streaming potential) is expressed in the study of landslides and is related to water circulation (Revil et al., 1999; Meric et al., 2006; Chambers et al., 2011). The advantage of this method is the low weight of the device and the possibility of covering large areas in a short time. Depending on the charge, electrical anomalies can be characteristic of either a draining and infiltration zone (negative charge) or an accumulation and upwelling of an impermeable zone (positive charge) (Aubert, 1997; Perrone et al., 2004; Chambers et al., 2011). In particular, previous works have shown that negative SP anomalies could correspond to a downward water movement in fractured surfaces or be related to an aquifer drawdown (Jardani et al., 2009; Sujitapan et al., 2019).

ERT and SP are frequently used together to delineate preferential flow paths (Titov et al., 2002; Lapenna et al., 2003; Jardani et al., 2006; Suski et al., 2006; Robert, 2012; Santoso et al., 2019). From a spatial point of view, the scope covered by a 2D electrical tomography survey is often limited to two-dimensional transects, which are often discontinuous despite possible overlaps. It does allow for in-depth imaging of the landslide structure and the limits of the vadose zone, even in complex formations and on hilly slopes. The SP allows the characterization

of the flow dynamics affecting a landslide over a continuous area, under the sole condition of accessibility. Therefore, it has the ability to validate and spatially extend the hydrogeological hypotheses made from ERT surveys by providing hydrokinetic information.

However, geophysical data must be used in conjunction with other investigative methods (Chambers et al., 2011; Perrone et al., 2014). In particular, they must be combined and calibrated with geological, geotechnical, and geomorphological data and observations to improve the interpretation reliability (Jongmans and Garambois, 2007). It is therefore important to couple data sets that are sometimes very heterogeneous. Geological and geomorphological knowledge is crucial for validating survey interpretations but also for assessing the observed phenomena and their functioning (Hearn and Hart, 2011). The study of hydrogeological behaviour also requires a focus on surface and subsurface flows. In this respect, hydrogeochemical analyses serve to highlight the internal mechanisms and the flow of water by studying, for example, major ions or physicochemical characteristics (Bogaard et al., 2004, 2007; Montety et al., 2007; Bertrand et al., 2013; Marc et al., 2017). Artificial and isotopic tracing techniques are also classically used to help dissociate the origin of waters in an unstable slope (Binet et al., 2007; Deiana et al., 2020).

The datasets to be integrated can be numerous and are sometime heterogeneous. The consistency of temporally and spatially disparate multi-source data with sometimes uneven reliability is an important issue for the characterization and conceptualization of landslide functioning (Bichler et al., 2004; Travelletti and Malet, 2012; Lissak et al., 2014b; Fressard et al., 2016; Denchik et al., 2019). This is particularly the case for long-term studied landslides, for which the data are sometimes discontinuous and scattered.

The study site discussed in this paper is a typical case of a complex landslide under hydrological control with a high sensitivity due to the presence of clays. One of its significant specificities is due to its coastal character. This site was the subject of several studies for more than 40 years, has been well documented and described from structural and kinematic points of view (Maquaire, 1990; Lissak, 2012). Although the hydrological influence on landslide activity has been proven, the hydrogeological functioning of the slope still begs many questions. The present research aims to improve the understanding of internal flows by the joint use of existing data sets (electrical tomography, geotechnical and geomorphological data), completed and supplemented by new investigations (self-potential and physicochemical studies of water). Thus, through an integrative multi-disciplinary approach, the objective is to homogenize this set of qualitative geotechnical, geophysical and hydrological data and analyse them to propose a new conceptual hydrogeological model.

The expected results from this work are manifold. It aims to (1) identify the preferred discharge locations from the continental water table; (2) understand the preferential water flows in the landslide; (3) highlight the degree of heterogeneity of the hydrogeological functioning of the site; and (4) establish a link between morpho-structural specificities and the behaviour of the landslide with regard to internal flows.

2. Description of the site and prior knowledge

2.1. Study site

The Cirque des Graves is located in the northern part of the Pays d'Auge (Normandy, France), along the coast of the English Channel. It is the largest of the four large landslides affecting the coastline between the municipalities of Trouville and Cricquebœuf (Fig. 1). These landslides are deep and rotational-translational and were initially triggered during the last Weichselian glaciations (Elhaï, 1963; Juignet et al., 1967; Journaux, 1971; Fressard, 2013). They are also all active due to the erosive action of the sea, exerting a continuous undermining effect and not allowing the slope to reach an equilibrium profile (Maquaire, 1990). This landslide of 47 ha (1 600 m long and 450 m wide) is adjacent to the Pays d'Auge plateau and surrounded by two non-permanent watercourses at its southwest and northeast boundaries. Its anthropization is recent as it dates back to the end of the 19th century (Lissak, 2012). Despite the destruction of a large part of the historical infrastructure due to previous accelerations, approximately twenty individual houses and a major tourist road (RD513) are still located on the unstable area.

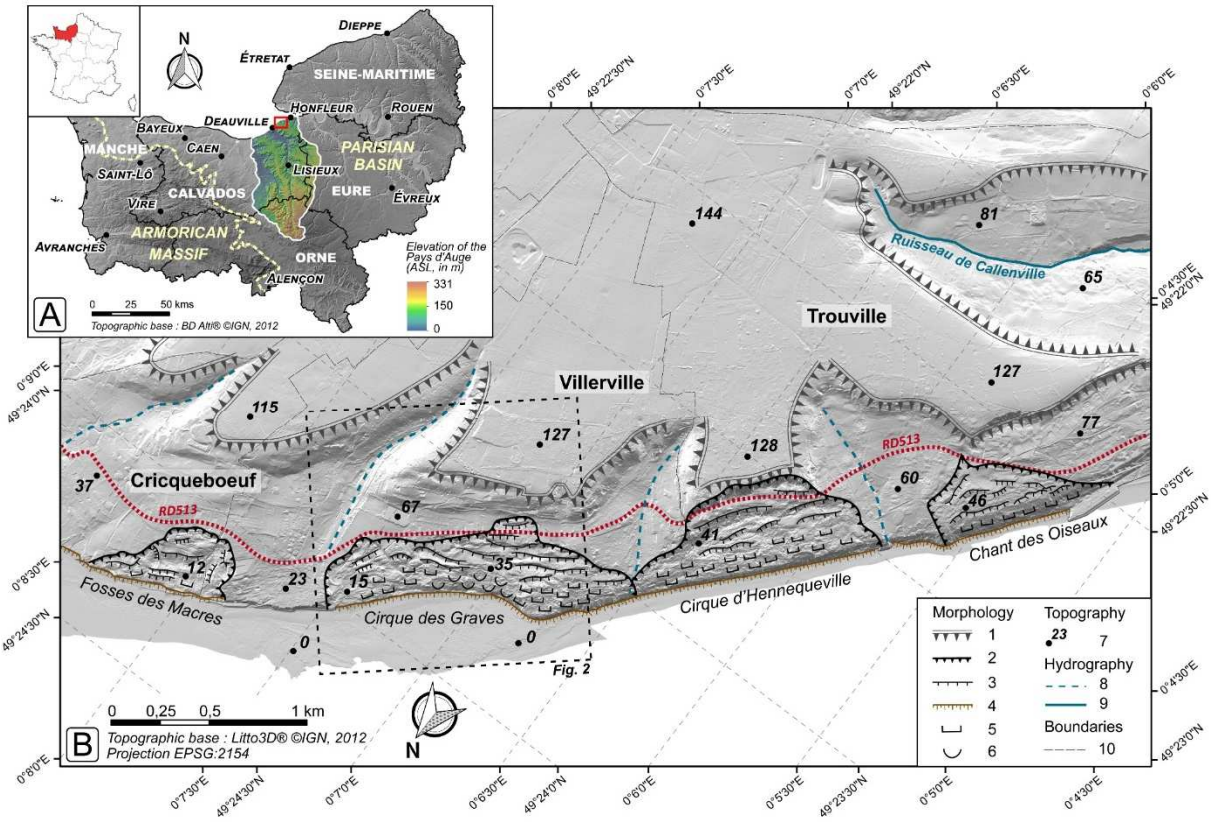

Fig. 1 – A: Location of the study field in Normandy; B: Morphological sketch of the four major coastal landsides of the Pays d'Auge, between Deauville and Honfleur. 1. Border of the Plateau d'Auge; 2. Main scarp of the landslides; 3. Secondary scarp; 4. Basal scarp; 5. Bumpy morphology; 6. Solifluction lobes morphology; 7. Spot height (in meters); 8. Temporary river flow; 9. Permanent river flow; 10. Municipality boundary.

The lithostructure of the unstable area is more complex than on the plateau due to the retrogressive kinematics of the slope generating discontinuities. From the plateau boundary to the sea, dissociated chalk slabs sink into Albian-Aptian sands and slide over Kimmeridgian and Oxfordian marly clay formations (Fig. 2). These formations, with fairly poor geotechnical characteristics, are underlain by a bedrock composed of Oxfordian gritty limestone (Maquaire, 1990). In the light of its size, the sharpness of the main scarp, the processes affecting the slope, and the landforms, this landslide can be classified as complex with rotational and translational components (Varnes, 1978; Cruden and Varnes, 1996; Lissak, 2012).

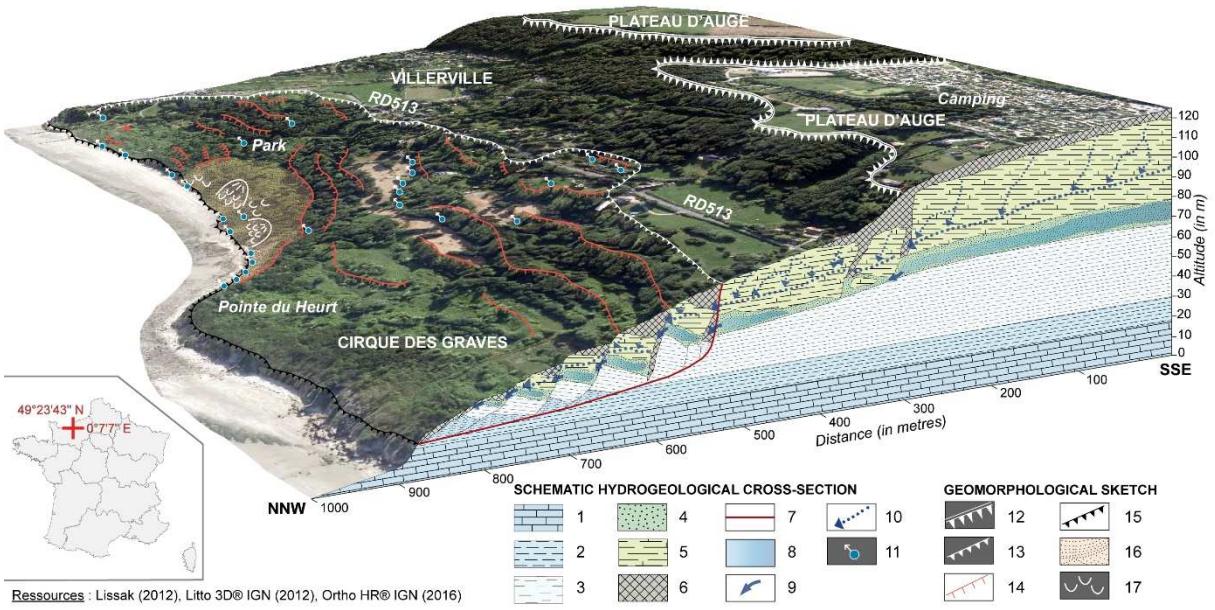

Fig. 2 – Schematic functioning of the Cirque des Graves proposed by Maquaire (1990) and Lissak (2012). 1. Oxfordian gritty limestone of Hennequeville; 2. Oxfordian clay of Villerville; 3. Kimmeridgian marl; 4. Albian sands; 5. Cenomanian chalk; 6. Surficial deposits (loess, colluvium, head); 7. Limit of the active landslide; 8. Albian sand groundwater; 9. Albian groundwater flow; 10. Cenomanian karstic flow; 11. Main springs; 12. Main scarp of the plateau; 13. Main scarp of the cirque (uphill limit of the landslide); 14. Secondary scarp; 15. Foot scarp; 16. Shallow landslide/muddy flow; 17. Denting and solifluxion.

2.2. Hydromechanical background

The first studies carried out in the Cirque des Graves date back to the 1930s, but a real research interest emerged after the major event of 1982 (Fig. 3 h) and focused on the geotechnical and kinematic response for better management of the infrastructure facilities (housing, networks, etc.). Since this first recent reactivation, three other events impacted the cirque in 1989, 1995 and 2001 (Maquaire, 1990; Lissak et al., 2013, 2014a; Costa et al., 2019).

Morpho-structural knowledge

The global structure of the landslide was determined thanks to numerous boreholes and geomorphological analyses (Maquaire, 1990; Lissak, 2012; Lissak et al., 2014b). In addition, electrical tomography surveys confirmed the thickness of the different features over 18 transects using vertical and horizontal variations in

resistivity (Lissak et al., 2014b).

The litho-stratigraphy is generally consistent with the morphological observations (Lissak et al., 2014b). The numerous main and secondary scarps, ranging in height from a few decimetres (Fig. 3 a) to more than 15 m upstream of the western part (Fig. 3 b, f), correspond to a segmentation of the chalk by weathering, inducing a dissociation into approximately 100 discrete slabs (Lissak, 2012; Lissak et al., 2014b). Their size increases from east to west (Lissak et al., 2014b). Tensile zones between the slabs are filled with silty-clay formations. Downwards, the thickness of the Albian-Aptian sands is uneven due to the importance of creep and the sinking of the chalk slabs in this loose and poorly cohesive horizon.

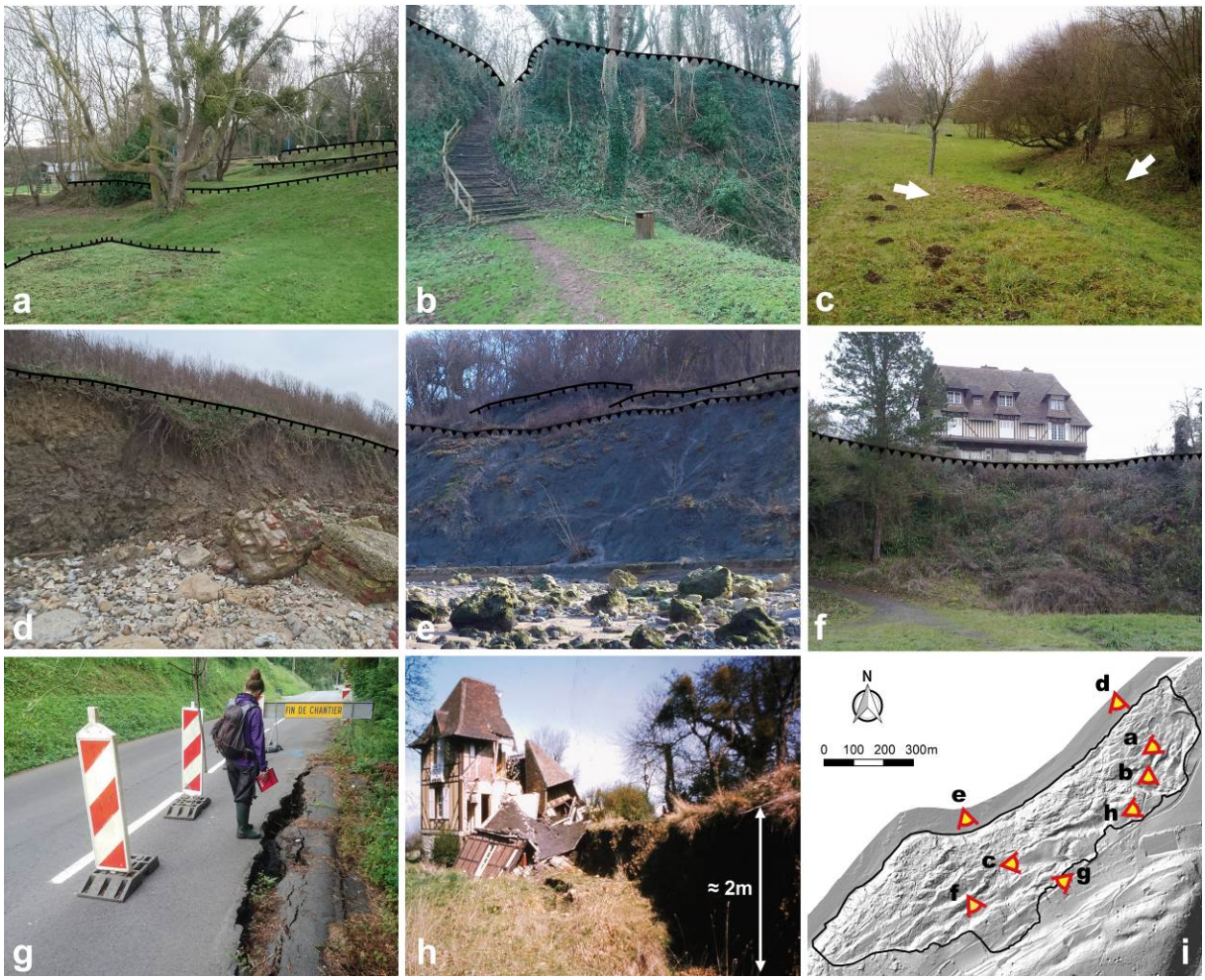

Fig. 3 – Main geomorphological features of the Cirque des Graves. (a) Minor scarp and stepped morphology in the park; (b) Major scarp (chalk outcrop) at the upstream part of the park (c) Slab tilted into a counter-slope at the centre of the landslide; (d) Heterogeneous soil matrix with blocks (heads) at the basal scarp of the park; (e) Mudflows in the Oxfordian marls at the foot of the landslide; (f) Building near a main scarp in the middle of the landslide; (g) Recent crack on the RD513 due to the

retreat of the main scarp; (h) Destruction of the villa Chanteclair after the acceleration of 1982 (Maquaire, 1984); (i) Location and orientation of the pictures.

The site is characterized by a chaotic morphology with a succession of scarps, counter-slopes, horst-graben structures, and general hummocky topography (Lissak et al., 2014b) (Fig. 3, b, c). The downstream part of the central and western areas is also characterized by the absence of chalk slabs (Fig. 8) and a solifluction dynamic of Oxfordian grey clays (Fig. 3 e).

The global volume of the slide was estimated at approximately $3e10^7$ m^3 (Lissak, 2012; Lissak et al., 2014b). The slip surfaces are deep, nested, and affect all of the horizons down to the Kimmeridgian and Oxfordian clays (Maquaire, 1990, 2000; Maquaire and Malet, 2007). The slip surface was characterized by inclinometric surveys to the east of the slide and measured at a depth of 23 m b.g.l. upstream and 5.5 m b.g.l. at the bottom of the slope (Maquaire, 1990). However, no inclinometer was able to characterize the deepest slip surface in the middle and western zones of the cirque because the devices were not implemented deep enough.

Kinematic knowledge

From a kinematic point of view, topographic monitoring was carried out using (1) a total station (Maquaire, 1990), (2) GPS monitoring on fixed benchmarks and (3) the implementation of permanent GNSS receivers (Lissak, 2012; Lissak et al., 2014a). These follow-ups revealed continuous activity with periodic accelerations and uneven dynamics (Maquaire, 1990; Lissak, 2012; Lissak et al., 2014b). The mean annual velocity ranges from 1-2 cm. yr^{-1} near the main scarp to 10-12 cm. yr^{-1} at the foot of the slope (Lissak, 2012). The most active zone is located at the foot of the middle zone, which is subject to clay mudflows (Fig. 3 e). The general dynamic is retrogressive with morphological downstream readjustments (Fig. 3 g), accentuated by basal sea excavation (Fig. 3 d, e).

Hydrological knowledge

Previous work has shown a direct link between the rise of the chalk water table on the Plateau d'Auge (at the Danestal piezometer, 17 km away from the slide) and the four major accelerations of 1982, 1989, 1995 and 2001

(Maquaire, 1990; Lissak, 2012; Bogaard et al., 2013; Lissak et al., 2014b; Costa et al., 2019) (Fig. 4). Although the levels between the plateau and the slope appear to be correlated, there is a delay of a few days to weeks due to the transit time of water through the matrix before the continental water table discharges on the coast (Lissak et al., 2014b).

Exceeding the trigger threshold to achieve a major acceleration requires several years with higher than normal annual rainfalls (Fig. 4 B). Thus, the major event of 1982 was preceded by six years of high annual precipitation. This expresses a cumulative effect of the precipitation on groundwater levels from one year to the next and underlines the major role of the continental discharge in exceeding the trigger levels (Maquaire, 2000).

Site-wide water flows are considered erratic with interconnected aquifers due to numerous structural discontinuities (Lafenetre, 2010; Lissak, 2012).

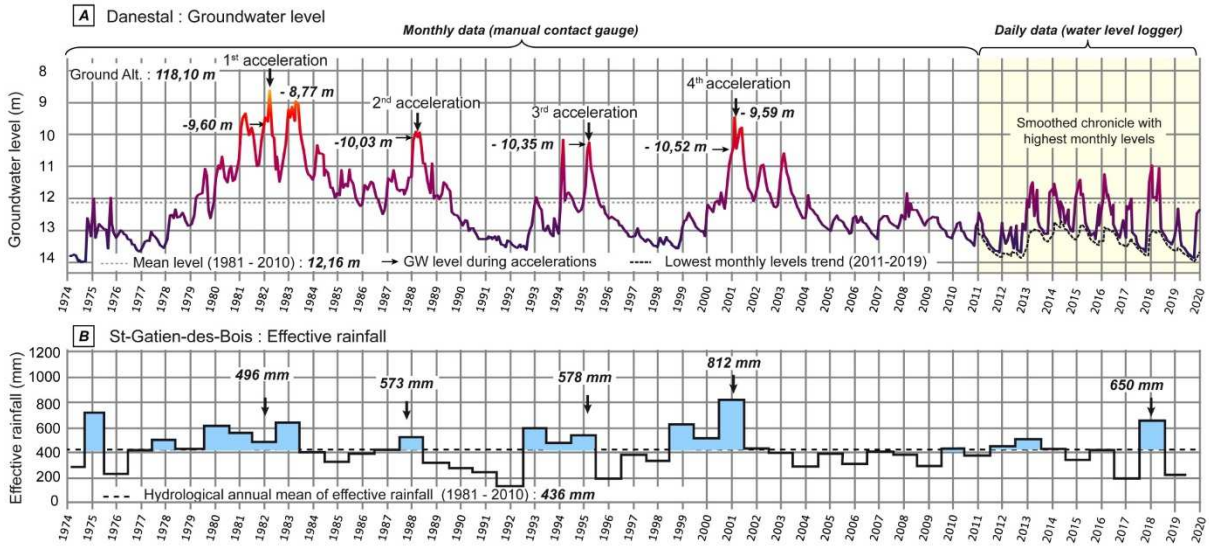

Fig. 4 – Correlation between the four major landslide accelerations in the Pays d'Auge and (A) the water table level at the Danestal piezometer. Because the chronicle is irregular from 2011 onwards (change of acquisition method), the data have been smoothed to show the extreme monthly levels; (B) the effective annual rainfall at the Météo-France weather station in St-Gatien-des-Bois, from 1974 to 2020 (updated from Lissak, 2012 and Costa et al., 2019).

The site has been equipped with a network of piezometers since the 1980s to allow groundwater monitoring. There is a slight temporal variability between high and low waters despite a significant spatial variability between some neighbouring piezometers that is directly related to the geological structure (Lissak, 2012).

Indeed, the hydraulic conductivity is variable depending on the material. Cohesive chalk and sandy formations are most permeable. Their values range from $1.5e^{-6}$ $m.s^{-1}$ to $1.8e^{-4}$ $m.s^{-1}$, while clays and surface flint clays have the weakest hydraulic conductivity of between $3.9e^{-9}$ $m.s^{-1}$ and $5.9e^{-7}$ $m.s^{-1}$ (Lafenetre, 2010; Lissak, 2012).

Hydromechanical modelling work has shown that a 1-m rise in the water table results in a 6% decrease in the overall safety factor of the slope (Maquaire, 2000; Maquaire and Malet, 2007). This demonstrates a real importance of the internal circulation of water on the landslide activity and confirms the hydrologically driven functioning of the slide.

3. Materials and methods

In light of the work described in the previous section, some data could be reused for joint analysis with the new investigations carried out. Fig. 5 shows the nature and location of all of the input data. The uneven spatial distribution of the data is partly due to the inaccessibility of part of the cirque (high scarps, fallow land, mudflow areas, etc.).

The methodological details for a re-analysis of the initial data and new hydrokinetic data are detailed hereafter by type of acquisition.

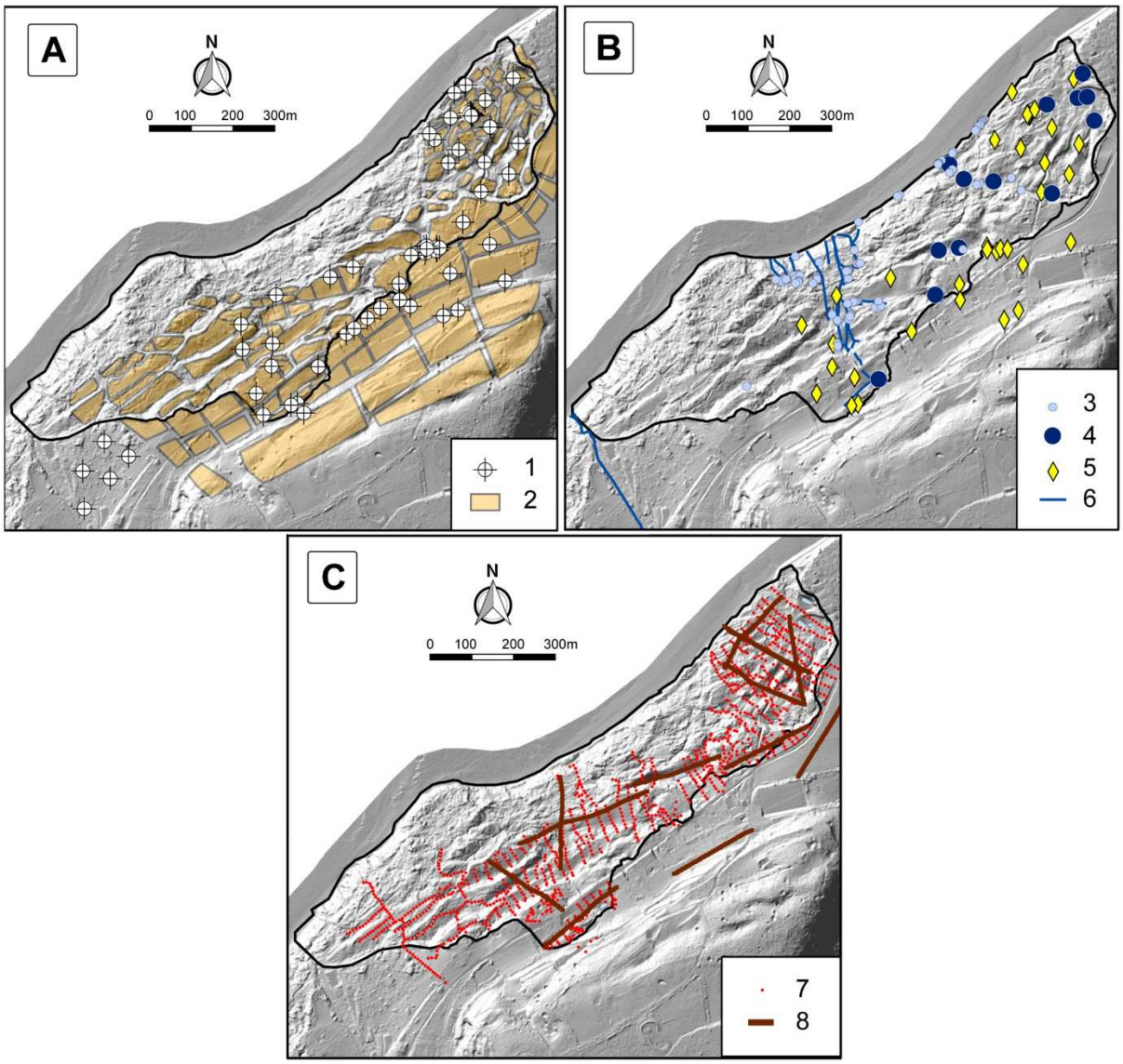

Fig. 5 – Typology and spatial distribution of the Cirque des Graves data used for morphostructural (A), hydrological (B) and geophysical (C) assessment. 1. Drillings from 1978 to 2019; 2. chalk compartment delineation (from Lissak, 2012); 3. spring/resurgence; 4. pond; 5. piezometric measurements; 6. drainage network; 7. SP measurement (2018 campaign); 8. ERT profile (2008/2009 survey).

3.1. Structural predisposition assessment

At first, our analysis consisted of synthesizing and reinterpreting borehole descriptions from multiple geotechnical analyses carried out since the 1970s. Logs of 62 boreholes drilled between 1978 and 2019 have been collected and used to assess the characteristics of the chalk (condition and thickness). These boreholes are mainly distributed in the eastern and upstream part of the site (Fig. 5A), characterizing the areas with stakes. One

issue was to dissociate the chalk and non-chalk horizons because saturated and weathered chalk is rarely described as such.

The assessment of chalk is crucial because thick and cohesive chalk generates cracks and sharp discontinuities. In the Cirque des Graves, these cracks are filled with heterogeneous and loose formations (Lissak, 2012). It significantly increases the transmissivity and recharge of aquifers (Foster and Milton, 1974). The transmissivity of a rock is defined by its void volume, which in turn depends on its matrix porosity and fissure porosity (Sausse, 1998). In the case of chalk, which is a material with low elasticity and subject to karstification, the fissure porosity can represent a significant part of the total flow. Therefore, this material illustrates heterogeneous behaviour (Buscarlet et al., 2011) with variable permeabilities and generally slow flow but also very localized fast flows (Crampon et al., 1993). This particular stratum is therefore critical for assessing the hydrogeological functioning of the slope.

3.2. Surface and groundwater study

Two physicochemical water characterization campaigns were carried out. The first one was conducted during a low water period (October 2018) and the second during a high water period (April 2019) to compare the results at hydrological extremes. The objective was to measure descriptive parameters such as water flow, pH index, conductivity and temperature in all ponds, springs and drained waters that were accessible and identified (Fig. 5B).

In situ measurements were performed using a TetraCon® 325 sensor for conductivity (± 1 $\mu S.cm^{-1}$) and a Sentix® 41 electrode for pH index (± 0.01) and temperature (± 0.1°C), which were both connected to a WTW® 340i measuring device (instruments by WTW® GmbH, Weilheim, Germany). Flow measurements were carried out by collecting water from springs and drains using suitable containers. The containers were filled over a stop-time period, and the quantities were measured in graduated test tubes. The locations of the measurement points were determined using a Trimble Juno 3B lightweight GPS field device.

These measurements allow for characterization of all areas where the aquifer is outcropping on the landslide. The locations of the measurement points were coupled to a set of 34 piezometric measurements carried out over the entire site. The currently operational network is composed of 13 piezometers and 7 inclinometers, followed by continuous piezometric sensors or a manual contact gauge. In addition, data from 14 other piezometric

measurement locations could be retrieved and integrated into the analysis. These data are partly from old piezometers no longer in use and partly from exploratory drilling enabling spot measurements of the groundwater level. The latter only provide point information on the piezometric levels. Because we know that the variations in the water table are low on a seasonal scale but exhibit strong site variability (Lafenetre, 2010; Lissak, 2012), it seems interesting to include them in the analysis.

The objective here is to characterize not the temporal variability but rather the spatial variability of the unconfined aquifer, which is directly related to the lithostructure. This is a first approach to try to highlight the preferential water flow paths over the unstable area.

A total of 97 groundwater measurements were used to produce a map of the mean piezometric surface. An ordinary kriging probabilistic interpolation method was applied, which considers the spatial dependency of the data while minimizing prediction errors (Matheron, 1963; Oliver and Webster, 1990; Baillargeon, 2005). This method is assumed to be suited to conventional hydrological problems (Gambolati and Volpi, 1979).

3.3. Geophysical imaging methods

Self-potential surveys

To refine internal flows, we used geophysical imaging tools. Self-potential is a suitable method for highlighting disturbances in electric currents and potential fields associated with water circulation (Gex, 1990; Naudet et al., 2008; Revil and Jardani, 2013). Natural electric fields originate directly from the infiltration of water through the process of electrofiltration. When water flows through a rock matrix, then the positive ions are fixed while the negative ones are carried away by the water. This creates an ion imbalance, which induces an electrical anomaly that can be measured by electrodes on the ground, thus making it possible to explain the orientation and intensity of the flow in said matrix (Naudet, 2004).

A self-potential mapping was carried out in April 2018 at the end of the high-water period. Some measurements have been performed using a Fluke175 high-impedance multimeter and two WM "Wolf LTD" ceramic electrodes saturated with Pb-PbCl liquid (lead-lead chloride), which cancels polarization effects. A total of 1,171 measurement points was realized with a fixed base configuration (one reference electrode and one moving electrode). The theoretical spacing of the survey was 10 m between each point on upstream-downstream profiles

and 25 m between two successive parallel profiles. Some adjustments had to be made according to accessibility conditions, particularly in the western zone of the landslide.

To avoid drifts due to the excessive distance between the electrodes, the location of the base station was shifted every five profiles (≈ 125 m). Between each base station, a measurement of the anomalies was made so that all values could be reported at the starting point of the survey. We also carried out numerous check points on the previous profiles each time that the base electrode location changed so that we can interconnect the survey lines and obtain a better monitoring of drifts and errors.

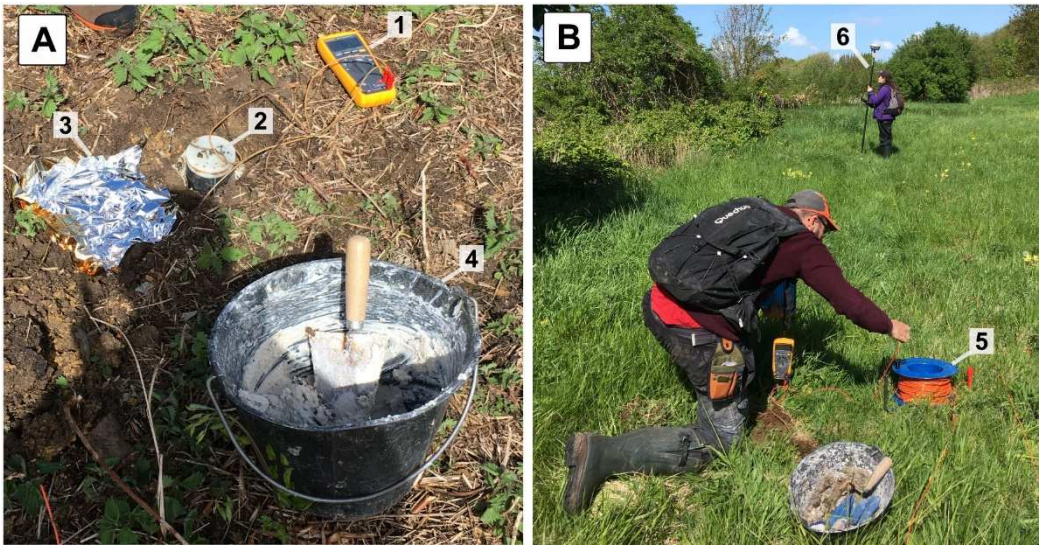

Fig. 6 – Self-potential device: (A) Derivation control between fixed and mobile electrode 1. High-impedance multimeter; 2. Mobile electrode; 3. Fixed electrode protected by the silver side of a survival blanket (to reflect solar radiation and limit the thermal drift). The blanket is then covered with clumps of earth during the survey; 4. Bucket with bentonite slurry. (B) Measurements of SP anomaly in the sliding area. 5. Cable reel connecting both electrodes; 6. GNSS acquisition to localize SP measurements.

The overall survey reference was located upstream of the park, outside of the unstable slope. We buried the fixed electrode 30 cm under the ground, protected from solar radiation to limit thermal drift or drifts due to ground drying (Fig. 6A).

Bentonite mud was systematically used to improve the electrical contact between the electrode and the ground. In addition, the positions of the measurement points were collected by GNSS surveying using a Trimble R8 differential GPS (Fig. 6B). 65% of the slide surface was covered, and the remaining 35% were not accessible.

A validation survey was conducted in April 2019 to check the reliability of the initial survey. To limit the acquisition time and the associated drifts, we chose to establish two lateral profiles and one longitudinal profile for a total of 225 measurement points.

All data points were interpolated using kriging, which is also a conventional and suitable method for interpolating geophysical data (Grandjean et al., 2006; Travelletti and Malet, 2012; Jaboyedoff et al., 2020). The regional model was filtered to eliminate the topographic effect and make local anomalies more apparent (Goto et al., 2012). The topographic influence was considered constant and calculated using a linear regression equation over all survey datapoints. This regression equation was applied to the DTM to define the theoretical influence of topography at each point of the raster. Finally, this influence was subtracted from the raster of measured raw anomalies.

Cross-analysis with ERT and geological data

In the second phase, the ERT campaign conducted in 2008-2009 in the frame of the SISCA project (Lissak et al., 2014b) was also reused. It aims to compare resistivity information, which depends on saturation and petrophysical characteristics, with hydrokinetic information from self-potential. The local materials of the Pays d'Auge are generally not very resistive. Chalk is above 60 Ω.m (Göktürkler et al., 2008; Naudet et al., 2008), while clays, sands and reworked materials are rather below 30 Ω.m (Perrone et al., 2004; Van Den Eeckhaut et al., 2007; Naudet et al., 2008; Jongmans et al., 2009; Sudha et al., 2009; Travelletti and Malet, 2012). Despite this slight distinction, the range of values makes it possible to discretize the lithofacies encountered.

Lissak et al. (2014b) identified a sharp contrast in resistivity with east-west growth explained by the litho-stratigraphy (Fig. 7). This observation is compared with the values and the type of underground flows highlighted by SP monitoring.

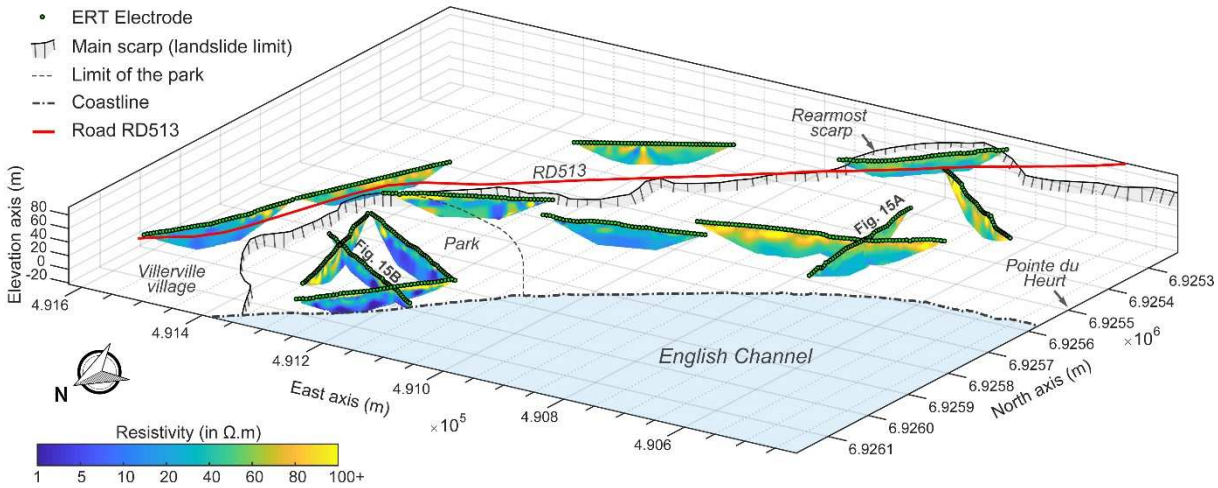

Fig. 7 – ERT inversion profiles from the previous geophysical campaign conducted in the frame of the SISCA project (2008). An east-west ascending gradient of resistivity values is observed.

A cross-interpretation work focused on two representative ERT profiles in the eastern and western parts of the landslide with an upstream-downstream orientation (located in Fig. 7). More information can be found in Lissak et al. (2014b) concerning the acquisition parameters and inversion processes of these ERT profiles. Drillings in the vicinity of these profiles were analysed so that they can contribute to the interpretation of these geophysical data.

4. Results

4.1. Structural analysis

The analysis of the 62 boreholes revealed a chalk thickness ranging from 2.80 m to 17.75 m (Fig. 8). The chalk layer is significantly thicker in the middle of the cirque, with a progressive decrease towards both extremities (northeast and southwest). The median zone includes the 14 drillings with the greatest thickness (>11 m).

The thinnest chalk layers are located in the northeast (park). In this zone, some drill logs do not clearly indicate the presence of chalk, even though the geomorphology suggests so. Out of a total of 20 drill holes, seven describe very significant weathering, most often referred to in descriptions as "yellowish-beige silty or sandy formations". This has been reinterpreted as "chalk", although the hydraulic conductivity of this altered material is closest to that of clay. The 13 other boreholes of the park did not identify any chalk, as the horizons were very heterometric with no clear distinction between the encountered facies.

The absence of obvious chalk is also possible elsewhere in the cirque. That is the case when the boreholes are located between compartments, in heterogeneous fill formations, or in the most reworked areas in the downstream part of the landslide.

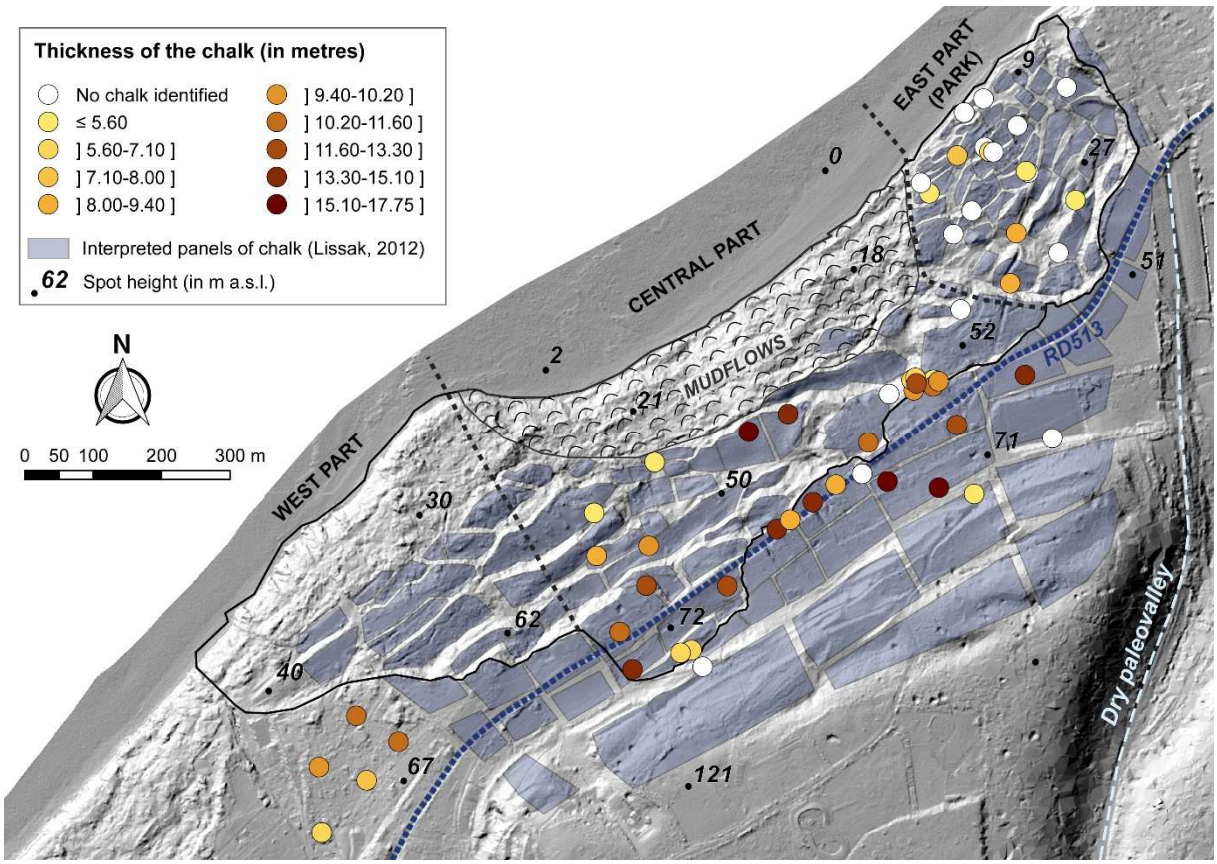

Fig. 8 – Variation of the chalk thickness from borehole logs in or nearby the Cirque des Graves and geometry of the identified slabs by Lissak, 2012

4.2. Characteristics of surface and underground waters

The physicochemical measurements reveal a concentration of the measured surface water in three sectors (Fig. 9). First, there is a significant flow at the southwestern border of the park along thalweg feeding ponds connected from the scarp. A large number of springs also outcrop at the foot of the chalk scarps in the middle of the cirque. Finally, a large number of springs, mainly in the form of seepage, can be observed at the point of contact between the Albian sands and clays, upstream of the mudflow area. Some springs outcrop directly on the foreshore, at the foot of the slope, in the heterogeneous reworked formations and heads, along the park's coastline. It is partly linked to the presence of flows at the park's boundary, located right on the upstream side.

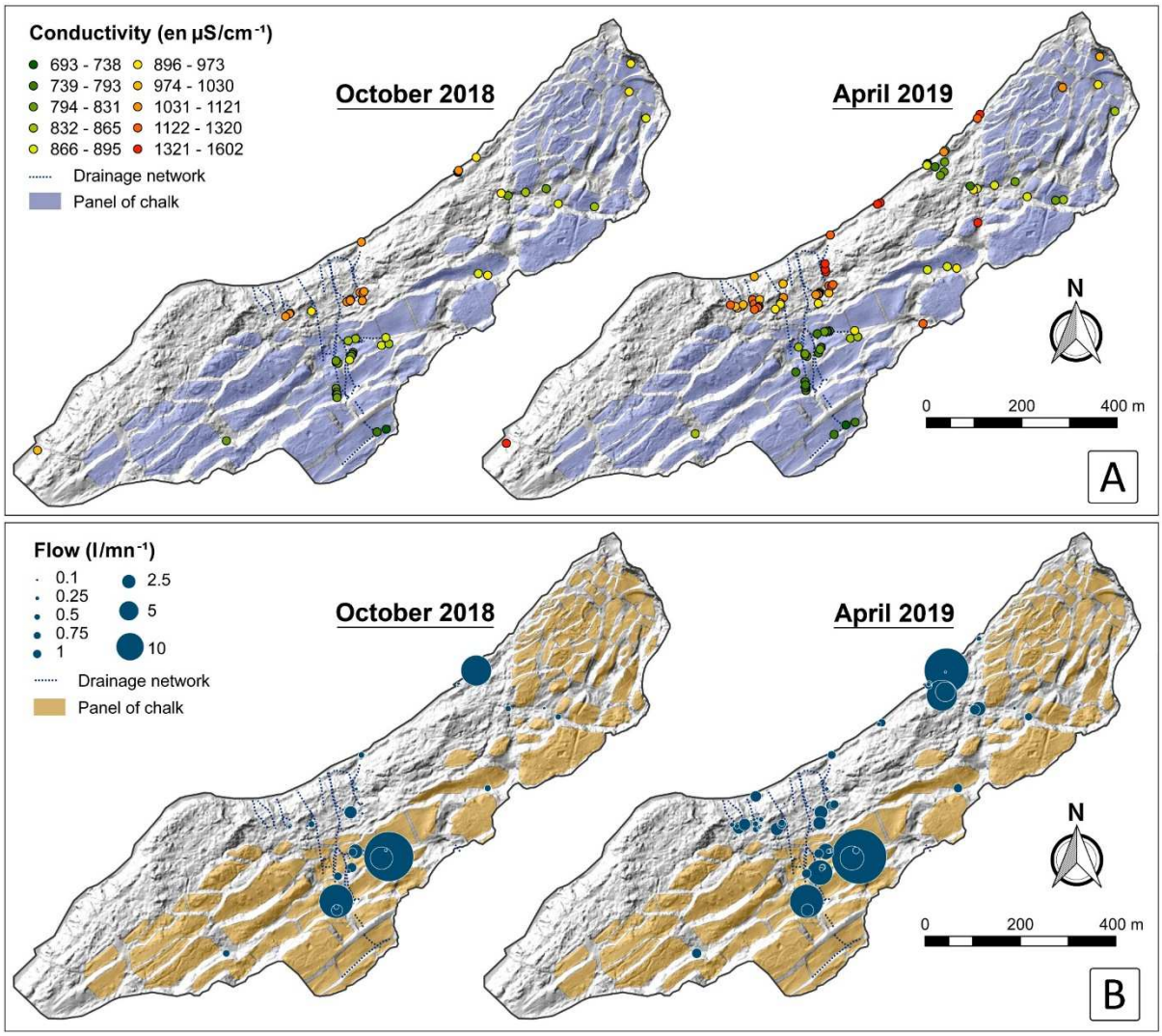

359

360 *Fig. 9 – (A) Conductivity measured in springs, ponds, and drains and (B) water flow measured in natural springs at the*
361 *Cirque des Graves during the field campaigns of October 2018 and April 2019*

362 The seasonality of the flows shows significant variations between October (low water) and April (high water). 39
363 additional measurement points were recorded during the high-water period, including 25 springs, 10 stagnant
364 areas, and 4 drains that had dried up by October 2018. The total flow measured at the springs increased from
365 115.0 l.min^{-1} to 171.80 l.min^{-1} (Table 1). The gap can be explained by an increase of 22.9 l.min^{-1} from the
366 springs already measured in low waters and is related to new resurgences for a total of 33.9 l.min^{-1}.

367 The spatial distribution highlights the importance of the central area on the measured flow (Fig. 9B), with 74%
368 of the total flow in October (85.1 l.min^{-1}) and 69% in April (119 l.min^{-1}). In this central area, a network of
369 artificial drainage is implemented to evacuate the excess of surface water through trenches, gullies and pipes
370 (Fig. 10B, C, D).

371 Electrical conductivity measurements increase from upstream to downstream and imply an ionic enrichment
372 (Fig. 9A). In low waters, the difference between the extreme values is 400 µS.cm^{-1} and rises to more than 700
373 µS.cm^{-1} in periods of high water. The nine springs with the highest values during the April 2019 survey are from
374 1321 to 1602 µS.cm^{-1} and were all dry in October 2018. They are also all located at the outcropping of sands,
375 after the last chalk slabs.

Measurements	**October 2018**	**April 2019**
Number of flowing springs	47	72
Number of ponds with stagnant water	8	18
Number of flowing drains	7	11
Temperature range (in °C)	12.0-20.3	9.3-17.7
Conductivity range (in µS.cm^{-1})	711-1103	693-1602
pH index range	6.68-8.55	7.19-8.58
Mean measured flow (l.mn^{-1})	2.52	2.59
Total measured flow (l.mn^{-1})	115	171.80

376 *Table 1 – Compared results between the two campaigns for surface water analysis*

377 Given the sedimentary context, waters logically tend to be basic. In both surveys, only one measuring point was
378 below pH 7. The October 2018 campaign reports an average pH of 7.74 compared to 7.82 in April 2019. The
379 variability is therefore low at the scale of the massif, with the lowest measurements systematically located in the
380 ponds, often eutrophicated with the presence of duckweed.

381 The variability of the temperature is related to the type of measurement. The lowest temperatures measured are
382 those of springs with an average of 14.9°C in October 2018 and 12.2°C in April 2019.

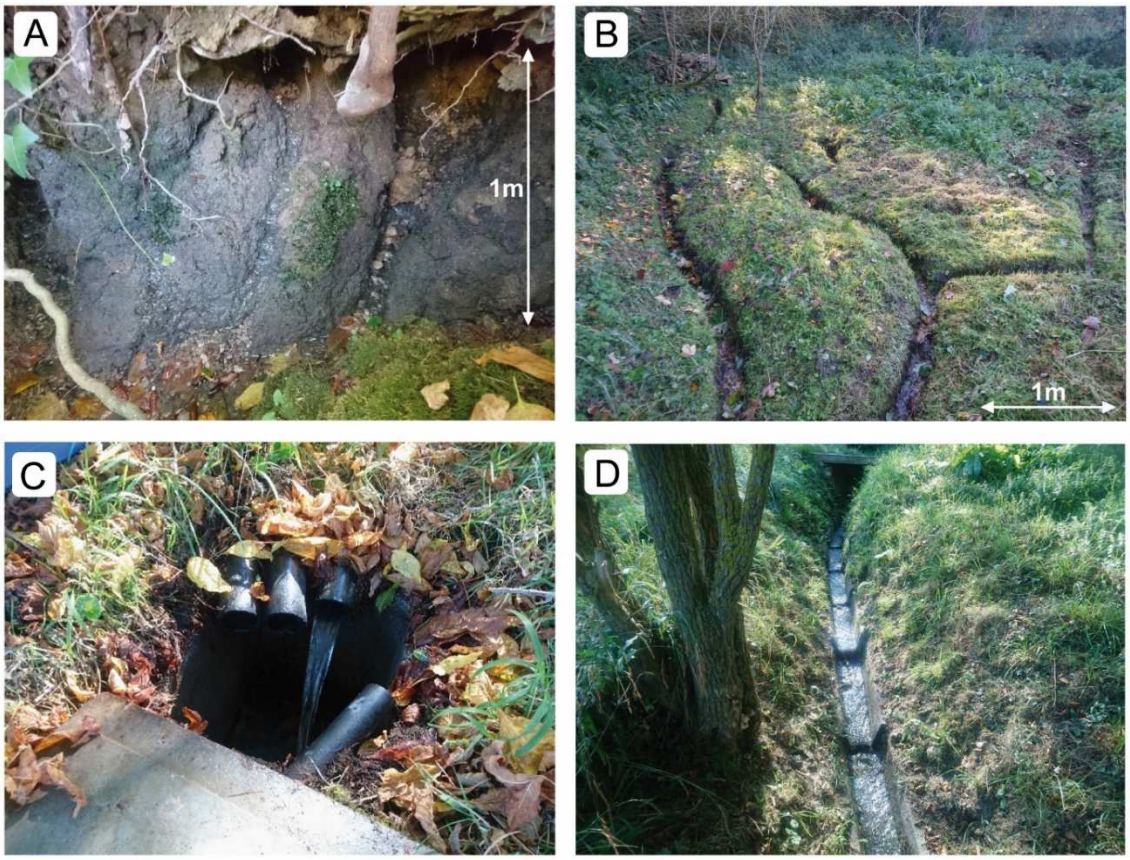

Fig. 10 – A: Natural spring from the Cenomanian chalk at the basis of a five-metre-deep scarp; B: Trenches dug in the soil to channel and drain surface waters; C: Water arrivals from four drainage pipes in a concrete manhole for recovery in a larger pipe; D: Open trench built with overlapped precast concrete elements

A piezometric map of the site has been produced by linking these measurement points with the piezometric data recorded (Fig. 11). The shallowest waters are located in the two areas of concentration characterized by numerous resurgences, with sub-surface levels of approximately 1 m in depth. In the unstable area, the water level seldom exceeds 5 to 7 m in depth. This water table depth increases in the upstream direction to reach up to 17 m near the plateau.

There is a slight edge effect due to overly large gaps, generating a "cluster effect" when the values are too different over a short distance. However, the deepest values located along the RD513 and generating theses clusters are indicative of a descending movement of the water in the filling materials in the cracks between chalk compartments, with values sometimes lower than 15 m b.g.l.$^{-1}$.

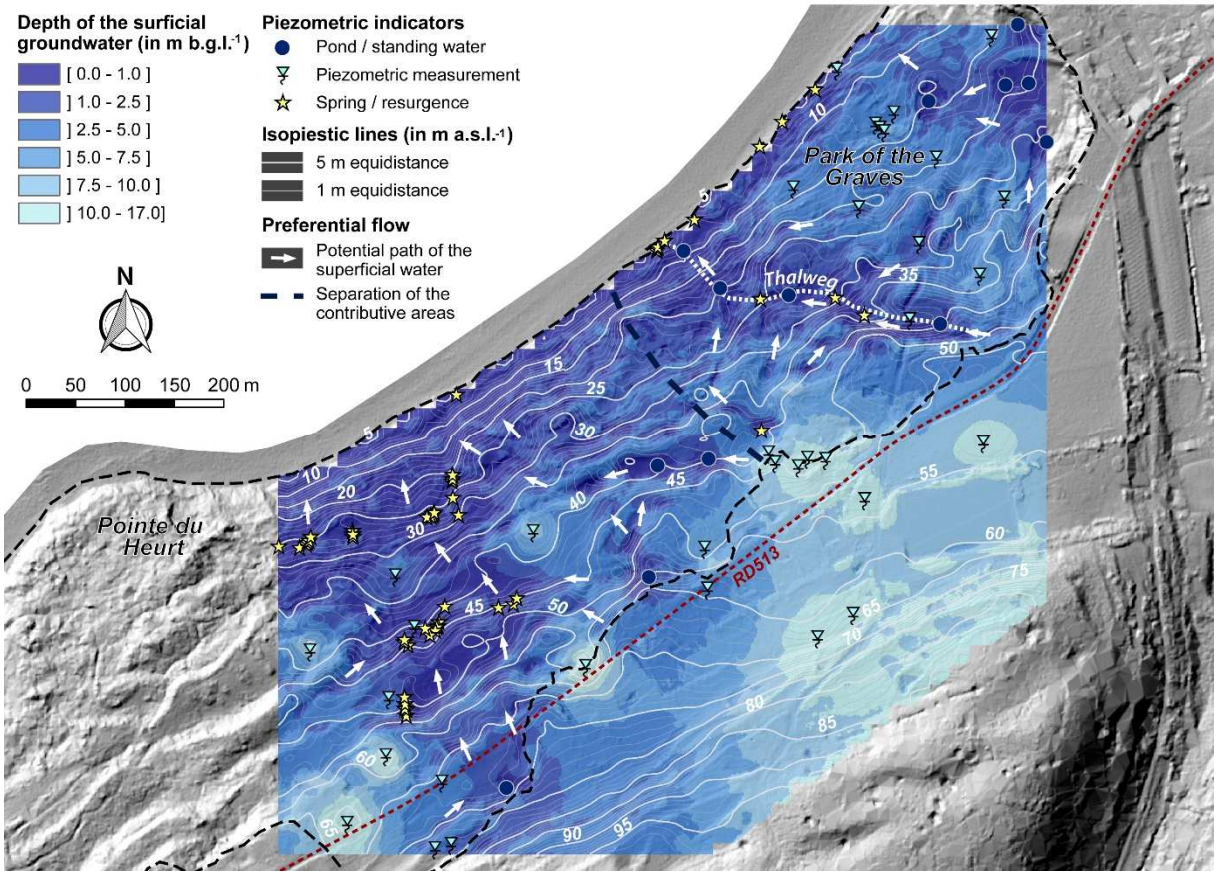

Fig. 11 - Piezometric level of the unconfined groundwater considering the identified pond, springs and piezometric information from piezometers and drilling descriptions

4.3. Hydrokinetic assessment based on geophysics

The interpolated SP map shows spatial heterogeneities (Fig. 12), with an increasing gradient of SP values from west to east. The range of values is quite limited, from -14.1 to +32.6 mV. The highest values are those found in the park, with values ranging from +3 to +32 mV, and no negative anomalies are found. The clusters having the highest values correspond to areas with springs and ponds (+20 to +32 mV). The maximum value of the entire survey was measured in the centre of a shallow pond located in this part of the cirque.

In the central section, the anomalies also increase from upstream to downstream, with marked negative values along the RD513 (-5 to -14 mV) and positive anomalies (+12 to +15 mV) at the contact of the clay-marl flows at the bottom of the slope. The upstream zone of the RD513 (in the centre of the landslide) corresponds to the strongest negative anomalies, near the main scarp.

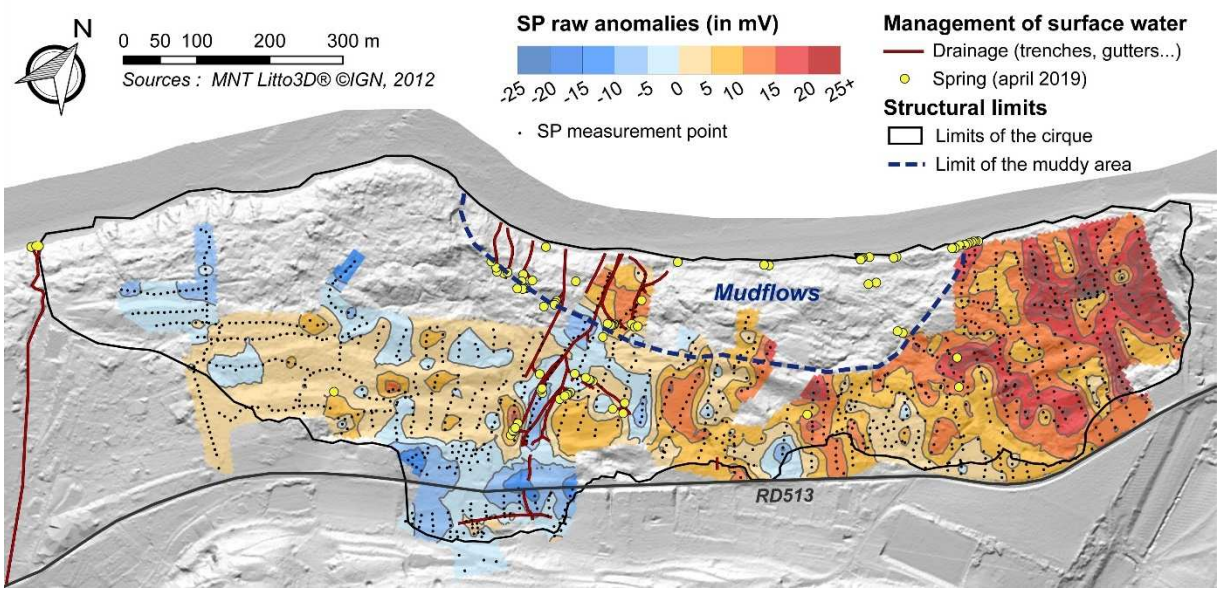

Fig. 12 – Interpolated map of the self-potential over the Cirque des Graves and location of major drains in the middle part of the landslide

A validation survey was conducted at the end of April 2019, in exactly the same period as the previous year, in an attempt to get as close as possible to the initial acquisition conditions. By relating the values from the second survey to the general reference from the first survey, the range of anomalies seems to be comparable in broader terms, ranging from -13.4 to +32.0 mV (Fig. 13A).

There are a few areas with deviations greater than 10 mV between the two surveys, which may be related to local changes in subsurface flows. However, the curves are comparable (Fig. 13B). The overall survey error is acceptable, with a median of 3.16 mV and a RMSE (Root Mean Square Error) of 2.14 mV.

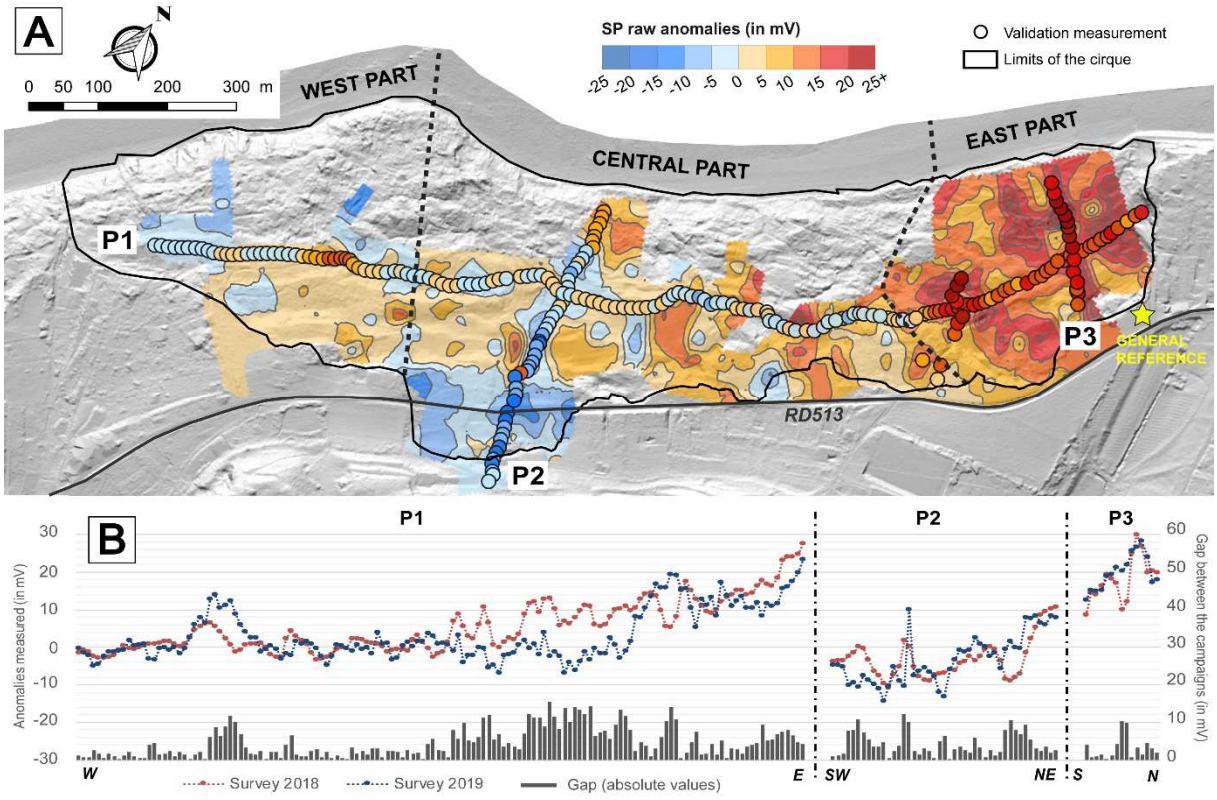

Fig. 13 – Comparison between the SP anomalies from the initial survey (2018) and those from the validation survey (2019). (A) Spatial distribution of the points of the three validation profiles superimposed on the initial raw anomaly map (the colour range is identical); (B) "Point to point" comparison between the 2018 raw anomaly map and the 2019 verification measurements for the three profiles. The grey bar graph represents the absolute gap between the campaigns.

Fig. 13 clearly shows the increase of anomalies from west to east and from upstream to downstream, thus highlighting a link with elevation following the same trends. The regional topographic effect was therefore filtered to more accurately reveal local anomalies (Fig. 14A) and was calculated to be -0.296 mV.m.

On the filtered map, the negative anomalies remain pronounced near the RD513 (≈ -10 mV) and are heightened around the drainage systems (from -10 to -20 mV). The western side of the Pointe du Heurt is marked by a progressive upstream-downstream gradient of anomalies, with the lowest values (-15 to -25 mV) in the direction of the cliff. In the park, slightly negative zones appear with an upstream-downstream decrease. However, this eastern area remains more characterized by positive anomalies up to +20 mV, particularly near the ponds and stagnant areas identified.

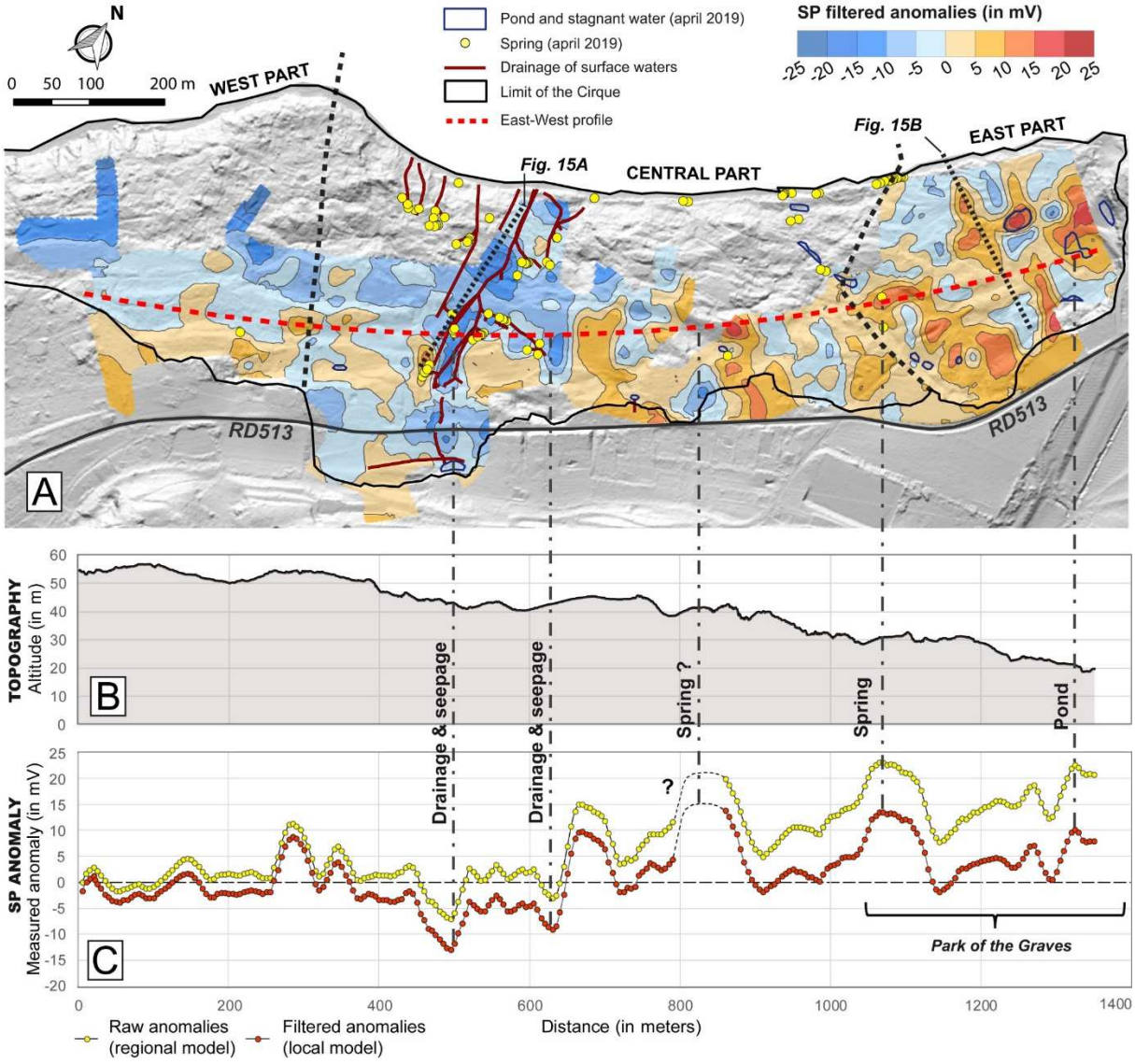

Fig. 14 – Filtering of the topographic effect on SP anomalies for the characterization of local hydrokinetic dynamics

To compare these surface acquisitions with in-depth information, two ERT profiles were selected and compared with nearby boreholes. These are respectively located in the park and in the central zone, above the mudflows (Fig. 15).

On the western profile (A), the SP anomalies decrease at the slope breaks. The upstream break shows a decrease of approximately 20 mV, and the anomaly reaches -18.5 mV in downstream direction. The flattened area in the middle of the profile also exhibits slightly less pronounced negative anomalies of up to -8 to -10 mV. Conversely, a positive anomaly located at the top of the profile reaches almost +12 mV in an area of stagnant water near springs. ERT and geology confirm these observations. The highest resistivities near the ground surface (50 to 500 Ω.m) are correlated with a fairly thick layer of chalk of up to ten metres. The contact with the

marls, constituting the lower limit of the aquifer formations, is identified at approximately 15 m in depth in borehole SC3 and coincides with resistivities below 30 Ω.m.

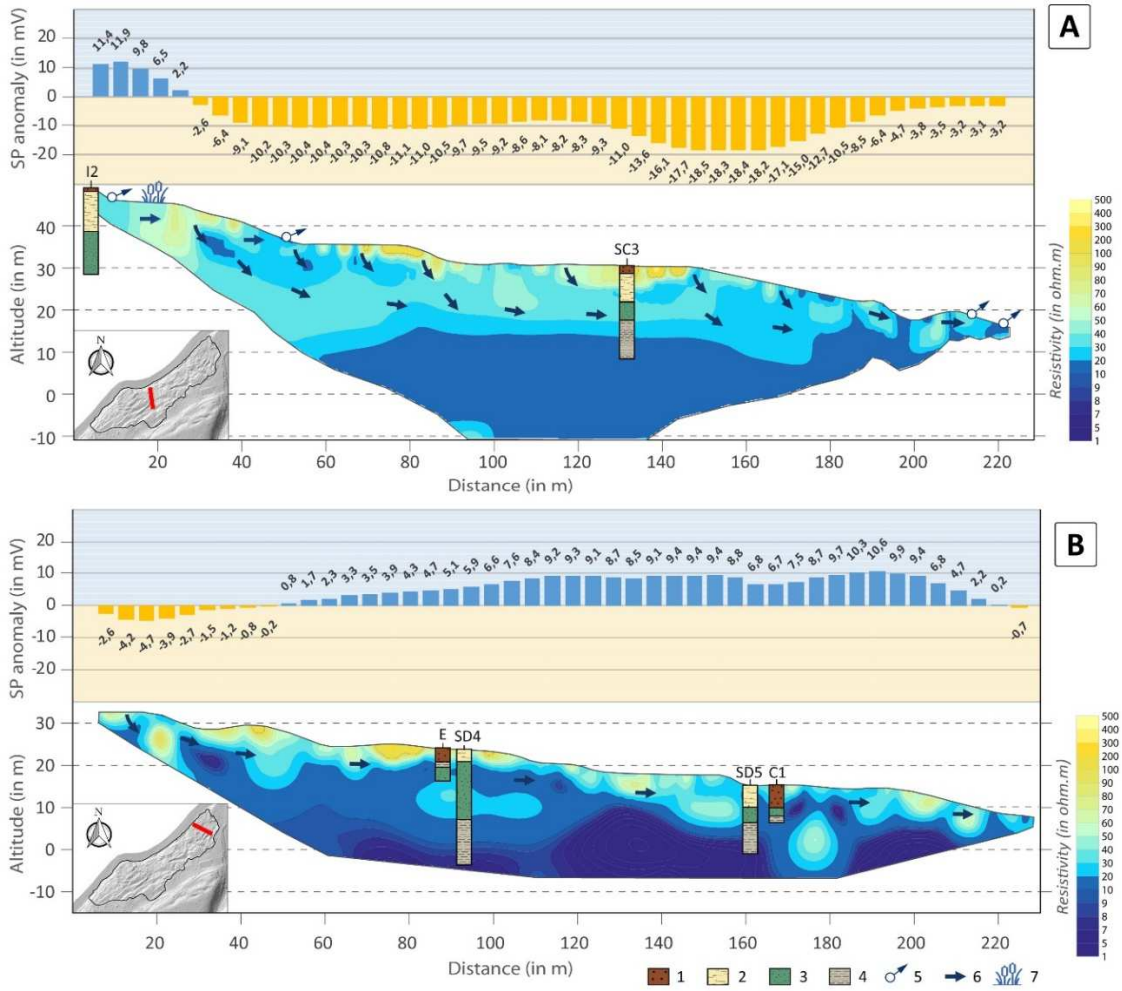

Fig. 15 – Correlation between SP filtered data (2018) and ERT profiles (2007-2008) in (A) the middle-western part of the Cirque and (B) in the eastern part of the Cirque (park). The location is specified in the thumbnail in the bottom left and corresponds to the two profiles indicated in Fig. 7 and Fig. 14. Legend: (1) Heterogeneous slope formation, (2) Chalk +/- weathered, (3) Glauconitic sand, (4) Clay & marl, (5) Spring, (6) Flow direction, (7) Stagnant water and hydrophilic vegetation.

On the eastern profile (B), weak negative anomalies (down to -4.7 mV) are observed upstream of the profile, in a zone located below the main scarp. The anomalies become positive and reach +10.6 mV in the last third of the slope. Lithologically, this zone is characterized by the splitting of weathered chalk slabs (boreholes SD4 and SD5), with a thickness ranging from 2 to 5 m. These slabs' fragments are interspersed with heterometric clay-loam slope formations (boreholes E and C1). The ERT also indicates fairly conductive layers (< 20 Ω.m) close to the ground surface. Near-surface resistivities are generally lower compared to the western side and barely exceed 70 Ω.m on a few isolated clusters, with a thickness that does not exceed 5 m.

5. Discussion

5.1. Towards a new hydrogeological model

Thanks to the characterization of the SP anomalies and the physicochemical analyses, we are able to propose hypotheses of spatial distribution, flow direction and intensity regarding the internal circulations, which could not have been done with the initial geometric model.

We are in a position to confirm the hypotheses of preferential discharge from the plateau. Alternately, the initial assumption of erratic flow and entanglement of the chalk and sand aquifers in the landslide is not confirmed throughout the unstable zone. The variations in water conductivity between the chalk and sand outcrops may suggest a partial dissociation of the aquifers in part of the slide.

The trend of the regional SP map is observed at a local scale, despite some infiltration zones that were not noticeable before the topographic filtering. It tends to show that topography is not solely responsible for the West-East increasing anomalies shown, with other electrokinetic sources being incriminated as the cause of these anomalies.

In light of these results, the three approaches (structural, hydrological and geophysical) converge towards the same trend, though with a division concerning the hydrogeological behaviour. Water flow dynamics are not homogeneous at the landslide scale, and it is possible to delineate three different compartments in the eastern, central and western parts of the landslide (Fig. 16). Such compartmentalization has already been performed for other landslides, such as the Super-Sauze earthflow (Malet, 2003; Malet et al., 2005; Montety et al., 2007). However, the use of SP provides essential information that allows the validation of the flow directions assumed from field surveys and laboratory data.

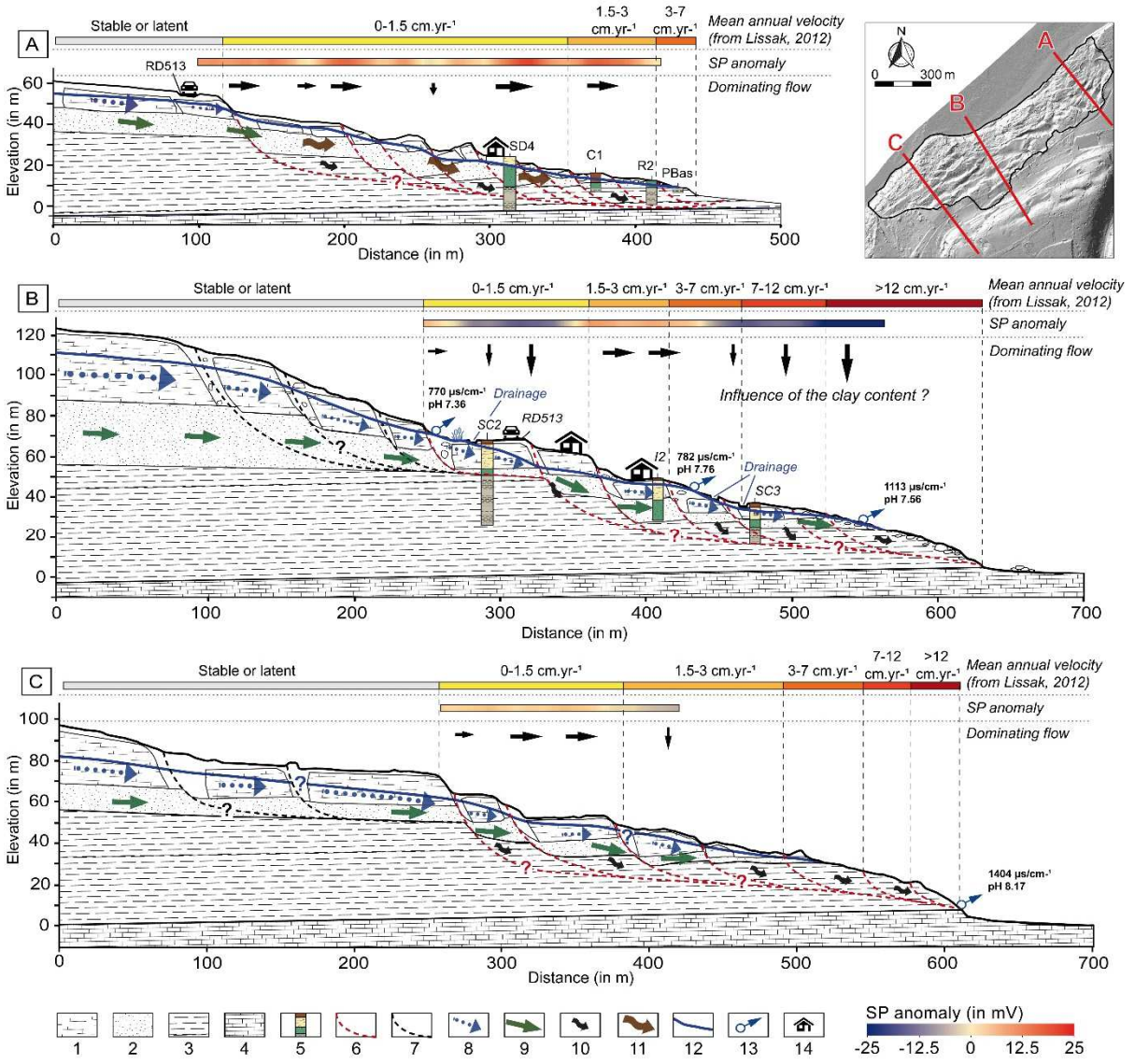

Fig. 16 – Cross-sections of the conceptual hydrogeological behaviour identified in each of the three parts of the cirque. Legend: (1) +/- weathered chalk, (2) glauconitic sands, (3) marls/clays, (4) gritty limestone, (5) boreholes, (6) potential active sliding surface, (7) potential latent sliding surface, (8) chalk water table flow, (9) sand water table flow, (10) clays/marls wetting, (11) undifferentiated matrix flow, (12) free water table level, (12) spring, (13) building.

Eastern Part

On the east side (park), the high permeability of the heterogeneous matrix, with thin and fragmented chalk slabs, facilitates the internal flow. These observations are validated by the geological descriptions and by the low resistivities up to near-surface. It explains the small number of resurgences in this zone, rather characterized by the presence of ponds, in relation to a near-surface water table level. In this zone, the groundwater seems to be undifferentiated in the sliding and heterogeneous matrix (Fig. 16 a). The surficial water supply from the Plateau

has been quantified with a continuous flow of water throughout the year, although the flow is quite limited. Even if the regional SP map (raw) shows no negative anomalies, the filtering map suggests the presence of some moderately infiltrated areas. Despite the eastward slight regional dip (1°), we detected no evidence of a direct inflow coming from the west of the cirque into the park. The thalweg delineating the park acts as a natural drain and allows the evacuation of a significant amount of water from springs and surface runoff. This area is also characterized by positive anomalies, consistent with water accumulation zones. This draining function is confirmed by the electrical conductivity values, which are steady from upstream to the foot of the slope, reflecting a continuous surface and sub-surface flow with the same origin.

Central Part

This central zone appears to be the main contributor of water inflows, which is confirmed by (1) the retrogressive saturated zone (pond and drains) behind the RD513; (2) the numerous springs found at mid-slope with high flow drained by hydraulic structures; and (3) the flow dynamics affecting the saturated clayey and marly materials at the bottom of the slope. This postulate was made by Lissak (2012), and the new acquisitions have improved this empirical knowledge and validated the assumed behaviour.

Field observations and negative SP anomalies express a main discharge from the plateau water table upstream of RD513, followed by a drawdown of the water table at the main scarp downstream of the road (Fig. 16 B). This discharge is probably amplified by the greater thickness of the aquiferous layers in the upstream zone, compared to the Eastern and Western areas. Such infiltration and SP anomalies in the detachment zone were noticed in other places, such as the Varco d'Izzo or Giarossa landslides (Lapenna et al., 2003; Perrone et al., 2004; Colangelo et al., 2006)

The flow appears less erratic in this part of the unstable zone, thanks to larger, thicker and generally less weathered chalk slabs, as shown by borehole logs, and higher resistivity values than in the park. Average water conductivities are measured at the top and middle of the slope (700-900 $\mu S.cm^{-1}$) at the chalk scarps, while a substantial increase occurs at the outcrop of the Albian sands down the slope. The values range from 900 to 1100 $\mu S.cm^{-1}$ in low waters and can reach 1600 $\mu S.cm^{-1}$ in high waters on springs that were initially dry in October. These high conductivities result in a decline in the SP anomaly, as the fluid conductivity decreases the electrokinetic coupling effect (Revil et al., 1999; Naudet et al., 2008).

526 The increase of the conductivity in a short distance could imply an extended residence time of these waters at the
527 outcrop and a possible dissociation between both aquifers. This hypothesis needs to be confirmed by means of
528 geochemical methods (major ions, isotopic or artificial tracing). Marine pollution due to sea spray also cannot be
529 excluded in a coastal context (Moore and Brunsden, 1996), and could influence these values, despite a dense tree
530 cover at the springs' location. Nevertheless, this influence seems limited, as suggested by the values measured at
531 the bottom of the thalweg delimiting the park, near the foreshore (± 800 $\mu S.cm^{-1}$).

532 In this area, the sand water table moistens the clays, which behave like an aquitard (i.e., weakly aquiferous but
533 containing an important quantity of water). This moistening, which induces an increase in pore pressure, is a
534 long process. The flow is delayed and dampened compared to a normal aquifer, given the low hydraulic
535 conductivity of clays (Tavenas and Leroueil, 1981). This process, associated with the discharge of the overlying
536 aquifers, explains the mudflow processes identified at the bottom of the slope.

537 Alternately, negative SP anomalies along the drainage systems have to be explained. These values are consistent
538 with the results of Bogoslovsky and Ogilvy (1973), which show a decrease in the SP values and negative
539 anomalies reaching -8 to -12 mV along ditches and channels. In general, the drainage structures increase the flow
540 velocity of groundwater and thus the electric fields of filtration. For Bogoslovsky and Ogilvy (1973), these
541 negative anomalies might be regarded as explaining a concentrated infiltration of water into the rock and are
542 therefore related to the efficiency of drainage or leakage due to the poor structural condition of the
543 developments. On the local network, this could be explained by seepage from trenches dug directly into the
544 ground or permeabilities at the junction of concrete elements forming part of the drainage network (Fig. 10).

545

546 ***Western Part***

547 The behaviour of the western part of the cirque (west of Pointe du Heurt) is not completely clear because the
548 available data set is more restricted in this area of the landslide due to the greater difficulty of access.

549 However, it is possible to define behavioural hypotheses from the few available data and field interpretations
550 (Fig. 16 C). The electrofiltration signal is quite heterogeneous from the raw results. However, there is a
551 decreasing gradient of SP anomalies in the direction of the foreshore, more clearly revealed by the filtering of the
552 topographic effect. For the upstream front, there are slightly positive anomalies (<10 mV), which may indicate a
553 weak surface discharge from the stable zone.

554 Thus, a decrease in anomalies towards the bottom of the slope could imply progressive water infiltration. Several
555 other observations mainly suggest deep-water functioning, such as: (1) the low number of resurgences and areas
556 of stagnation (springs and ponds); (2) the high scarps in this area (>15 m); and (3) permanent flows with high
557 conductivity (1003 Ω.m in autumn and 1404 Ω.m in spring) at the contact with the Villerville marls on the cliff
558 edge involving a rather long residence time. The significant decrease in the downstream SP values may also be
559 influenced by the change in substrate, with the clay-marl facies outcropping on the lower half of the slope of this
560 western zone. Indeed, the soil resistivity distribution controls the amplitude of the self-potential anomaly. Clay is
561 characterized by a very low resistivity (visible with ERT) and does not favour the occurrence of strong SP
562 anomalies (Skianis, 2012).

563

564 **5.2. Interpretation limits and errors in the SP survey**

565 Aubert (1997) points out an insufficient knowledge of the generation of SP potentials, which makes the
566 interpretation complicated and requires case-by-case argumentation. Over the years, the improvements of this
567 knowledge made it a powerful and proven method for solving hydrogeological problems (Naudet and Binley,
568 2006). However, many parameters may explain the SP signal, defined by Hämmann et al. (1997) as an overlay
569 of elementary sources. It is therefore crucial to consider data processing and interpretations in the environmental
570 context.

571 For example, SP can help to determine the piezometric level by inverting the self-potential values (Darnet et al.,
572 2003; Naudet, 2004; Naudet and Binley, 2006), which is not appropriate in our case due to the topography and
573 very rugged geology of the area. A bivariate analysis between SP anomalies and measured piezometric levels
574 shows a total absence of correlation with R^2=0.027. The electrofiltration anomalies measured in our case seem to
575 be mainly influenced by water infiltrations and accumulations. We have therefore limited our approach to the
576 identification and mapping of the main upward or downward preferential flow paths, which brings to light the
577 discharge zones and the deep or surficial behaviour. This geophysical method requires a-priori information on
578 the distribution of cross-coupling and the origin of primary electric field sources (Hämmann et al., 1997), which
579 is enabled by the hydromechanical information from in situ surveys.

580 A discussion regarding data quality is necessary to determine the robustness of the survey. Electrical drifts occur
581 between the two electrodes during the survey depending on many local factors, such as thermal variations, soil
582 drying, vegetation suction or local disturbance signals (e.g., power lines, pipes). It is therefore necessary to check

583 the drift regularly during the survey. We carried out 46 control measurements during the campaign by checking
584 the electrical potential difference between the two electrodes at the location of the reference electrode or by
585 monitoring the drift over time at the location of the measurement points.

586 The distribution of the control measures reveals discrepancies that need to be analysed. The range of absolute
587 deviations between initial and control measurements is from 0.0 to 17 mV. The RMSE of the distribution is 2.32
588 mV, and the standard deviation is 5.07 mV. The difference between the RMSE and standard deviation is large,
589 which tends to confirm the influence of the few extreme values, with the RMSE being less sensitive to these
590 values (Bouthevillain and Mathis, 1995). These extremes may be related to local factors that may generate
591 disturbances of the measurable electric field at the surface, as mentioned above. It is also important to note that
592 the drift is relative to the size of the study area (cumulative effect at each base change) and the duration of the
593 monitoring (time-varying effect of soil properties) (Corwin and Ward, 1990). We investigated 47 ha over 12
594 days in dry conditions, with more than a thousand measurement points, which is significant compared to
595 conventional landslide surveys.

596 Previous work has shown similar errors. For example, a standard deviation in the range of ± 10-15 mV was
597 reported by Naudet (2004); ± 20 mV was reported by Fournier (1989); ± 10 mV was reported by Birch (1993); ±
598 5 mV was reported by Corwin and Hoover (1979), Perry et al. (1996), Panthulu et al. (2001), and Revil et al.
599 (2004); and ± 3 mV was reported by Hämmann et al. (1997). The main difference with the current study is the
600 range of values, which remains quite small, of the order of a few tens of mV, probably influenced by the clayey
601 substrate. Comparatively, the range of values was approximately 600 mV for Naudet (2004) or 900 mV for
602 Fournier (1989) and Revil et al. (2004) but in different environments or with different scientific issues (e.g.,
603 pollutant dispersion).

604 The maximum drift of the survey is 17 mV and corresponds to 48.7 % of the total range of measured values (0-
605 34.9 mV), while the root mean square error is only 6.6 % of this range. The errors in the estimation of
606 geophysical surveys carried out in a natural environment are generally of the order of 20 %, a value that is
607 considered by geophysicists as a tolerance threshold (Abdul Samad, 2017). Therefore, excluding the few extreme
608 ones, the highlighted errors seem to be acceptable.

609

610

6. Conclusion

The objective of this study was to assess the hydrogeologic behaviour of the Cirque des Graves using spatially and temporally heterogeneous datasets to improve the limited initial knowledge. Structural and piezometric datasets acquired over the long term were first used to assess the predisposition of the massif to underground flows. This allows the highlighting of litho-stratigraphic disparities explaining contrasts regarding water table levels and the distribution of runoffs on the surface. The wide heterogeneity of the geological formations encountered (variation in thickness, reworking and discontinuities due to landslide dynamics, varying density and hydraulic conductivity of the materials, etc.) therefore explains the uneven functioning of the slope. Second, geophysical and physicochemical data acquisition aimed to explain this variability by characterizing the hydrokinetics of the slope.

We have shown that the slope is divided into three compartments with an east-west division. The eastern part (park) is characterized by a heterogeneous matrix with weathered and fractured chalk slabs favouring the mixing of the two water tables of chalk and sand. These observations are verified by (1) the borehole logs, (2) a low electrical conductivity of the matrix to the near surface, (3) the low number of resurgences despite a high water table, (4) a homogeneous water conductivity from upstream to downstream, and (5) the quite positive SP anomalies despite some small infiltration zones identified after the removal of the regional topographic effect.

Conversely, the central part is characterized by a less linear and more marked flow (upstream pond, numerous resurgences and drainage networks). This is due to more pronounced scarps enhancing transmissivity along slip surfaces and a thicker, less weathered chalk, which is confirmed by geological logs and ERT. Regarding the hydrokinetic features, the numerous SP anomalies support the hypotheses of (1) a greater verticality of the flows than in the east, (2) an inflow of the continental water table upstream and then an infiltration in the vicinity of the RD513, and (3) an incomplete dissociation of the chalk and sand aquifers. The influence of the drainage networks on the electrofiltration phenomena is also clearly noticeable.

Finally, the west of the Pointe du Heurt, while less characterized, is fairly close to the central zone from a structural point of view but seems to experience infiltration with less intense water inflows than the central area, as shown by the low number of resurgences and decreasing SP anomalies towards the shore.

In the end, the implementation of boreholes and piezometers are classical methods of investigations for monitoring unstable slopes. Based on this available empirical knowledge concerning numerous landslides, the results obtained show that hydrogeological knowledge can be substantially improved with light, easily

transportable investigation methods and with limited costs, even on large and complex slopes. In non-homogeneous environments, ERT and SP are recognized as the two easiest geophysical methods to implement (Meric et al., 2006) and are interesting to couple. The acquisition of physicochemical parameters is also simple and inexpensive.

However, the observed conductivity measurements open up new research prospects. Further research would be required to dissociate the contributions between the two aquifers of chalk and sand in a reliable manner and to determine what comes under the impluvium. Knowledge of residence times would also help with interpretation. To that end, the study of the strontium isotopic ratio $87^{Sr}/86^{Sr}$ could be used (Siegel et al., 2000; Legeay, 2013) to determine the level of connection between the two regional aquifers at a local scale (Brenot et al., 2008).

Other geophysical methods should also be explored. The international literature shows recent developments in terms of SP data processing, which may allow for more advanced acquisitions and data inversions for future studies but is beyond the main focus of the present paper. For example, continuous SP monitoring could be processed over a given period (from several hours to several months) to characterize the variability of groundwater flows (Meric, 2006). The realization of self-potential tomograms (Patella, 1997) would also be considered and has already proved its worth in landslide studies (Perrone et al., 2004; Colangelo et al., 2006).

Acknowledgements

This research was supported by the ANR project “RICOCHET: Multi-risk assessment on coastal territory in a global change context (2017-2021)” (ANR-16-CE03-0008), funded by the French National Research Agency (ANR). This work was also conducted with the help of data collected during the ANR Risk-Nat project “SISCA: Integrated Monitoring System of landslide crises (e.g., acceleration, fluidization of large muddy landslides) (2009-2011)” (ANR- 08-RISKNAT-009).

The Villerville landslide, locally managed by LETG-Caen laboratory, is a permanent site instrumented as part of the OMIV-INSU observatory (French Observatory on Landslides) led by the EOST laboratory at the University of Strasbourg.

The authors thank all of the contributors to this work during the field campaigns from the LETG-Caen and BRGM teams. We also express our gratitude to the three anonymous reviewers for their constructive comments and suggestions, which helped to improve the paper.

References

Abdul Samad, F., 2017. Polarisation Provoquée : expérimentation, modélisation et applications géophysiques (thèse de doctorat en Géophysique appliquée). Université Pierre et Marie Curie.

Aubert, M., 1997. Application de la mesure des potentiels électriques de polarisation spontanée (PS) à la reconnaissance des formations superficielles. Actes du colloque GEOFCAN, Géophysique des sols et des formations superficielles 121–126.

Baillargeon, S., 2005. Le krigeage: revue de la théorie et application à l'interpolation spatiale de données de précipitations (mémoire de la faculté des études supérieures de l'Université Laval).

Bertrand, C., Marc, V., Vallet, A., Mudry, J., Schmitt, A.-D., 2013. Apport de l'hydrogéochimie pour la caractérisation des mouvements gravitaires. JAG – 3èmes Journées Aléas Gravitaires, Grenoble, France 8 p.

Bichler, A., Bobrowsky, P., Best, M., Douma, M., Hunter, J., Calvert, T., Burns, R., 2004. Three-dimensional mapping of a landslide using a multi-geophysical approach: the Quesnel Forks landslide. Landslides 1, 29–40. https://doi.org/10.1007/s10346-003-0008-7

Binet, S., Jomard, H., Lebourg, T., Guglielmi, Y., Tric, E., Bertrand, C., Mudry, J., 2007. Experimental analysis of groundwater flow through a landslide slip surface using natural and artificial water chemical tracers. Hydrol. Process. 21, 3463–3472. https://doi.org/10.1002/hyp.6579

Birch, F., 1993. Testing Fournier's method for finding water table from self-potential. Groundwater 31, 50–56.

Bogaard, T., Guglielmi, Y., Marc, V., Emblanch, C., Bertrand, C., Mudry, J., 2007. Hydrogeochemistry in landslide research: a review. Bulletin de la Societe Geologique de France 178, 113–126. https://doi.org/10.2113/gssgfbull.178.2.113

Bogaard, T., Maharjan, L.D., Maquaire, O., Lissak, C., Malet, J.-P., 2013. Identification of Hydro-Meteorological Triggers for Villerville Coastal Landslide, in: Margottini, C., Canuti, P., Sassa, K. (Eds.), Landslide Science and Practice. Springer Berlin Heidelberg, Berlin, Heidelberg, pp. 141–145. https://doi.org/10.1007/978-3-642-31427-8_18

Bogaard, T.A., Buma, J.T., Klawer, C.J.M., 2004. Testing the potential of geochemical techniques for identifying hydrological systems within landslides in partly weathered marls. Geomorphology 58, 323–338. https://doi.org/10.1016/j.geomorph.2003.08.001

Bogoslovsky, V., Ogilvy, A., 1977. Geophysical methods for the investigation of landslides. Geophysics 42, 562–571.

Bogoslovsky, V.V., Ogilvy, A.A., 1973. Deformations of natural electric fields near drainage structures. Geophys Prospect 21, 716–723. https://doi.org/10.1111/j.1365-2478.1973.tb00053.x

Bouthevillain, K., Mathis, A., 1995. Prévisions : mesures, erreurs et principaux résultats. estat 285, 89–100. https://doi.org/10.3406/estat.1995.5982

Brenot, A., Baran, N., Petelet-Giraud, E., Négrel, P., 2008. Interaction between different water bodies in a small catchment in the Paris basin (Brévilles, France): Tracing of multiple Sr sources through Sr isotopes coupled with Mg/Sr and Ca/Sr ratios. Applied Geochemistry 23, 58–75. https://doi.org/10.1016/j.apgeochem.2007.09.006

Buscarlet, P., Pickaert, L., Stollsteiner, P., Klinka, T., Wuilleumier, A., Asfirane, F., 2011. Modélisation de la nappe de la craie – Calage du modèle hydrodynamique en régime transitoire – Rapport d'avancement BRGM/RP-60217-FR, 46 p., 25 fig., 4 tab., 2 annexes.

Caris, J., Van Asch, T.W., 1991. Geophysical, geotechnical and hydrological investigations of a small landslide in the French Alps. Engineering Geology 31, 249–276.

Chambers, J.E., Wilkinson, P.B., Kuras, O., Ford, J.R., Gunn, D.A., Meldrum, P.I., Pennington, C.V.L., Weller, A.L., Hobbs, P.R.N., Ogilvy, R.D., 2011. Three-dimensional geophysical anatomy of an active landslide in Lias Group mudrocks, Cleveland Basin, UK. Geomorphology 125, 472–484. https://doi.org/10.1016/j.geomorph.2010.09.017

Cherubini, A., 2019. Utilisation des méthodes de polarisation spontanée et polarisation provoquée pour la détection de CO_2 en milieu poreux carbonaté (thèse de doctorat en Sciences de la Terre). Université Bordeaux Montaigne.

Colangelo, G., Lapenna, V., Perrone, A., Piscitelli, S., Telesca, L., 2006. 2D Self-Potential tomographies for studying groundwater flows in the Varco d'Izzo landslide (Basilicata, southern Italy). Engineering Geology 88, 274–286. https://doi.org/10.1016/j.enggeo.2006.09.014

Corwin, R.F., Hoover, D.B., 1979. The self-potential method in geothermal exploration. Geophysics 44, 226–245.

Corwin, R.F., Ward, S., 1990. The self-potential method for environmental and engineering applications. Geotechnical and environmental geophysics 1, 127–145.

Costa, S., Maquaire, O., Letortu, P., Thirard, G., Compain, V., Roulland, T., Medjkane, M., Davidson, R., Graff, K., Lissak, C., Delacourt, C., Duguet, T., Fauchard, C., Antoine, R., 2019. Sedimentary Coastal Cliffs of Normandy: Modalities and Quantification of Retreat. Journal of Coastal Research 88, 46. https://doi.org/10.2112/SI88-005.1

Coulouma, G., Samyn, K., Grandjean, G., Follain, S., Lagacherie, P., 2012. Combining seismic and electric methods for predicting bedrock depth along a Mediterranean soil toposequence. Geoderma 170, 39–47. https://doi.org/10.1016/j.geoderma.2011.11.015

Crampon, N., Roux, J.-C., Bracq, P., 1993. Hydrogéologie de la craie en France. Hydrogéologie (Orléans) 81–123.

Cruden, D.M., Varnes, D.J., 1996. Landslides: investigation and mitigation. Chapter 3-Landslide types and processes. Transportation research board special report.

Darnet, M., Marquis, G., Sailhac, P., 2003. Estimating aquifer hydraulic properties from the inversion of surface Streaming Potential (SP) anomalies: characterizing aquifer from SP inversion. Geophys. Res. Lett. 30. https://doi.org/10.1029/2003GL017631

Deiana, M., Mussi, M., Pennisi, M., Boccolari, M., Corsini, A., Ronchetti, F., 2020. Contribution of water geochemistry and isotopes (δ18O, δ2H, 3H, 87Sr/86Sr and δ11B) to the study of groundwater flow properties and underlying bedrock structures of a deep landslide. Environ Earth Sci 79, 30. https://doi.org/10.1007/s12665-019-8772-4

Denchik, N., Gautier, S., Dupuy, M., Batiot-Guilhe, C., Lopez, M., Léonardi, V., Geeraert, M., Henry, G., Neyens, D., Coudray, P., Pezard, P.A., 2019. In-situ geophysical and hydro-geochemical monitoring to infer landslide dynamics (Pégairolles-de-l'Escalette landslide, France). Engineering Geology 254, 102–112. https://doi.org/10.1016/j.enggeo.2019.04.009

Di Maio, R., De Paola, C., Forte, G., Piegari, E., Pirone, M., Santo, A., Urciuoli, G., 2020. An integrated geological, geotechnical and geophysical approach to identify predisposing factors for flowslide occurrence. Engineering Geology 267, 105473.

Ekinci, Y.L., Türkeş, M., Demirci, A., Erginal, A.E., 2013. Shallow and deep-seated regolith slides on deforested slopes in Çanakkale, NW Turkey. Geomorphology 201, 70–79. https://doi.org/10.1016/j.geomorph.2013.06.008

Elhaï, H., 1963. La Normandie occidentale entre la Seine et le golfe normand-breton. Etude morphologique (Thèse d'Etat). Université de Paris, imprimerie Bière, Bordeaux.

Erginal, A.E., Öztürk, B., Ekinci, Y.L., Demirci, A., 2009. Investigation of the nature of slip surface using geochemical analyses and 2-D electrical resistivity tomography: a case study from Lapseki area, NW Turkey. Environ Geol 58, 1167. https://doi.org/10.1007/s00254-008-1594-4

Foster, S.S.D., Milton, V.A., 1974. The permeability and storage of an unconfined Chalk aquifer. IAHS Hydrol. Sci. Bull 19, 485–500.

Fournier, C., 1989. Spontaneous potentials and resistivity surveys applied to hydrogeology in a volcanic area: case history of the chaine des puys (Puy-de-Dôme, France). Geophys Prospect 37, 647–668. https://doi.org/10.1111/j.1365-2478.1989.tb02228.x

Frappa, M., Lebourg, T., 2001. Mesures géophysiques pour l'analyse des glissements de terrain. Rev. Fr. Geotech. 33–39. https://doi.org/10.1051/geotech/2001095033

Fressard, M., 2013. Les glissements de terrain du Pays d'Auge continental (Normandie, France) Caractérisation, cartographie, analyse spatiale et modélisation (Thèse de géographie). Université de Caen.

Fressard, M., Maquaire, O., Thiery, Y., Davidson, R., Lissak, C., 2016. Multi-method characterisation of an active landslide: Case study in the Pays d'Auge plateau (Normandy, France). Geomorphology 270, 22–39. https://doi.org/10.1016/j.geomorph.2016.07.001

Gambolati, G., Volpi, G., 1979. A conceptual deterministic analysis of the kriging technique in hydrology. Water Resour. Res. 15, 625–629. https://doi.org/10.1029/WR015i003p00625

Gance, J., Malet, J.-P., Supper, R., Sailhac, P., Ottowitz, D., Jochum, B., 2016. Permanent electrical resistivity measurements for monitoring water circulation in clayey landslides. Journal of Applied Geophysics 126, 98–115. https://doi.org/10.1016/j.jappgeo.2016.01.011

Gex, P., 1990. Acquisition et interprétation des données de polarisation spontanée, bibliographie générale sur les potentiels spontanés, Bulletin IGL. Institut de géophysique-Université de Lausanne.

Godio, A., Strobbia, C., De Bacco, G., 2006. Geophysical characterisation of a rockslide in an alpine region. Engineering Geology 83, 273–286. https://doi.org/10.1016/j.enggeo.2005.06.034

Göktürkler, G., Balkaya, Ç., Erhan, Z., Yurdakul, A., 2008. Investigation of a shallow alluvial aquifer using geoelectrical methods: a case from Turkey. Environ Geol 54, 1283–1290. https://doi.org/10.1007/s00254-007-0911-7

Goto, T., Kondo, K., Ito, R., Esaki, K., Oouchi, Y., Abe, Y., Tsujimura, M., 2012. Implications of Self-Potential Distribution for Groundwater Flow System in a Nonvolcanic Mountain Slope. International Journal of Geophysics 2012, 1–10. https://doi.org/10.1155/2012/640250

Grandjean, G., Pennetier, C., Bitri, A., Meric, O., Malet, J.-P., 2006. Caractérisation de la structure interne et de l'état hydrique de glissements argilo-marneux par tomographie géophysique : l'exemple du glissement-coulée de Super-Sauze (Alpes du Sud, France). Comptes Rendus Geoscience 338, 587–595. https://doi.org/10.1016/j.crte.2006.03.013

Hack, H.R.G.K., 2020. Weathering, Erosion, and Susceptibility to Weathering, in: Kanji, M., He, M., Ribeiro e Sousa, L. (Eds.), Soft Rock Mechanics and Engineering. Springer International Publishing, Cham, pp. 291–333. https://doi.org/10.1007/978-3-030-29477-9_11

Hämmann, M., Maurer, H.R., Green, A.G., Horstmeyer, H., 1997. Self-Potential Image Reconstruction: Capabilities and Limitations. JEEG 2, 21–35. https://doi.org/10.4133/JEEG2.1.21

Hearn, G.J., Hart, A.B., 2011. Geomorphological Contributions to Landslide Risk Assessment, in: Developments in Earth Surface Processes. Elsevier, pp. 107–148. https://doi.org/10.1016/B978-0-444-53446-0.00005-7

Jaboyedoff, M., Baillifard, F., Couture, R., Locat, J., Locat, P., 2004. Toward preliminary hazard assessment using DEM topographic analysis and simple mechanical modeling by means of sloping local base level. Landslides: evaluation and stabilization. Balkema, Taylor & Francis Group, London 199–206.

Jaboyedoff, M., Carrea, D., Derron, M.-H., Oppikofer, T., Penna, I.M., Rudaz, B., 2020. A review of methods used to estimate initial landslide failure surface depths and volumes. Engineering Geology 267, 105478. https://doi.org/10.1016/j.enggeo.2020.105478

Jaboyedoff, M., Couture, R., Locat, P., 2009. Structural analysis of Turtle Mountain (Alberta) using digital elevation model: toward a progressive failure. Geomorphology 103, 5–16.

Jardani, A., Revil, A., Akoa, F., Schmutz, M., Florsch, N., Dupont, J.P., 2006. Least squares inversion of self-potential (SP) data and application to the shallow flow of ground water in sinkholes. Geophys. Res. Lett. 33, L19306. https://doi.org/10.1029/2006GL027458

Jardani, A., Revil, A., Barrash, W., Crespy, A., Rizzo, E., Straface, S., Cardiff, M., Malama, B., Miller, C., Johnson, T., 2009. Reconstruction of the Water Table from Self-Potential Data: A Bayesian Approach. Ground Water 47, 213–227. https://doi.org/10.1111/j.1745-6584.2008.00513.x

Jomard, H., Lebourg, T., Binet, S., Tric, E., Hernandez, M., 2007. Characterization of an internal slope movement structure by hydrogeophysical surveying. Terra Nova 19, 48–57. https://doi.org/10.1111/j.1365-3121.2006.00712.x

Jongmans, D., Bièvre, G., Renalier, F., Schwartz, S., Beaurez, N., Orengo, Y., 2009. Geophysical investigation of a large landslide in glaciolacustrine clays in the Trièves area (French Alps). Engineering Geology 109, 45–56. https://doi.org/10.1016/j.enggeo.2008.10.005

Jongmans, D., Garambois, S., 2007. Geophysical investigation of landslides : a review. Bulletin de la Societe Geologique de France 178, 101–112. https://doi.org/10.2113/gssgfbull.178.2.101

Journaux, A., 1971. Formations superficielles et dynamique des versants dans le pays d'Auge. Presented at the Colloque International de Géomorphologie, Réunion de la commission d'études des formations superficielles et de la dynamique des versants du Comité National de Géographie, Excursion dans le Pays d'Auge, p. 27.

Juignet, P., Pannetier, J., Payren, C., 1967. Sur la présence du Turonien dans la vallée de la Touques entre Pont-l'Evêque et Coquainvillers et sur quelques exemples spectaculaires de glissement en masse. Bulletin de la société linnéenne de Normandie 8 (2), 213–224.

Kearey, P., Brooks, M., Hill, I., 2002. An introduction to geophysical exploration 3rd ed. Hong Kong: Blackwell.

Lafenetre, S., 2010. Étude hydrogéologique d'un versant instable : cas des glissements de terrain de Villerville-Cricqueboeuf, Calvados, Basse-Normandie (Mémoire de Master 1). Université d'Avignon et des Pays du Vaucluse, Avignon, France.

Lapenna, V., Lorenzo, P., Perrone, A., Piscitelli, S., Sdao, F., Rizzo, E., 2003. High-resolution geoelectrical tomographies in the study of Giarrossa landslide (southern Italy). Bulletin of Engineering Geology and the Environment 62, 259–268. https://doi.org/10.1007/s10064-002-0184-z

Lee, C.-C., Yang, C.-H., Liu, H.-C., Wen, K.-L., Wang, Z.-B., Chen, Y.-J., 2008. A Study of the hydrogeological environment of the lishan landslide area using resistivity image profiling and borehole data. Engineering Geology 98, 115–125.

Legeay, P.-L., 2013. Utilisation des isotopes du strontium pour caractériser les dynamiques de recharge et de transfert d'un aquifère karstique (Mémoire de master 2 « Sciences de l'Univers, Environnement, Ecologie »). Université Pierre et Marie Curie, Paris.

Lissak, C., 2012. Les glissements de terrain des versants côtiers du Pays d'Auge (Calvados) : Morphologie, fonctionnement et gestion du risque. (Thèse de géographie). Université de Caen, Caen, France.

Lissak, C., Maquaire, O., Davidson, R., Malet, J.-P., 2014a. Piezometric thresholds for triggering landslides along the Normandy coast, France. Geomorphologie 20, 145–158. https://doi.org/10.4000/geomorphologie.10607

Lissak, C., Maquaire, O., Malet, J.-P., Bitri, A., Samyn, K., Grandjean, G., Bourdeau, C., Reiffsteck, P., Davidson, R., 2014b. Airborne and ground-based data sources for characterizing the morpho-structure of a coastal landslide. Geomorphology 217, 140–151. https://doi.org/10.1016/j.geomorph.2014.04.019

Lissak, C., Maquaire, O., Puissant, A., Malet, J.-P., 2013. Landslide consequences and post crisis management along the coastal slopes of Normandy, France, in: Landslide Science and Practice. Springer, pp. 23–30.

Malet, J.-P., 2003. Les 'glissements de type écoulement' dans les marnes noires des Alpes du Sud. Morphologie, fonctionnement et modélisation hydro-mécanique (Thèse de doctorat). Université Louis Pasteur-Strasbourg I.

Malet, J.-P., van Asch, Th.W.J., van Beek, R., Maquaire, O., 2005. Forecasting the behaviour of complex landslides with a spatially distributed hydrological model. Nat. Hazards Earth Syst. Sci. 5, 71–85. https://doi.org/10.5194/nhess-5-71-2005

Maquaire, O., 2000. Effects of groundwater on the Villerville-Cricqueboeuf landslides. Sixteen years of survey (Calvados, France). Presented at the 8th Landslides International symposium, Cardiff, pp. 1005–1010.

Maquaire, O., 1990. Les mouvements de terrain de la côte du Calvados: recherche et prévention. Editions du BRGM, vol. 197.

Maquaire, O., Malet, J.-P., 2007. Assessment of coastal landslide hazard: the Villerville-Cricqueboeuf landslides (Normandy coast, France). Presented at the European Geosciences Union.

Marc, V., Bertrand, C., Malet, J.-P., Carry, N., Simler, R., Cervi, F., 2017. Groundwater-Surface waters interactions at slope and catchment scales: implications for landsliding in clay-rich slopes: Hydrochemistry and geochemical modelling to infer groundwater flows. Hydrol. Process. 31, 364–381. https://doi.org/10.1002/hyp.11030

Matheron, G., 1963. Principles of geostatistics. Economic Geology 58, 1246–1266. https://doi.org/10.2113/gsecongeo.58.8.1246

Meric, O., 2006. Étude de mouvements de terrain par méthodes géophysiques (Thèse de géophysique). Université Joseph-Fourier - Grenoble I.

Meric, O., Garambois, S., Jongmans, D., Wathelet, M., Chatelain, J.L., Vengeon, J.M., 2005. Application of geophysical methods for the investigation of the large gravitational mass movement of Séchilienne, France. Can. Geotech. J. 42, 1105–1115. https://doi.org/10.1139/t05-034

Meric, O., Garambois, S., Orengo, Y., 2006. Large gravitational movement monitoring using a spontaneous potential network. Presented at the 19th EEGS Symposium on the Application of Geophysics to Engineering and Environmental Problems, European Association of Geoscientists & Engineers, p. cp-181.

Montety, V. de, Marc, V., Emblanch, C., Malet, J.-P., Bertrand, C., Maquaire, O., Bogaard, T.A., 2007. Identifying the origin of groundwater and flow processes in complex landslides affecting black marls: insights from a hydrochemical survey. Earth Surf. Process. Landforms 32, 32–48. https://doi.org/10.1002/esp.1370

Moore, R., Brunsden, D., 1996. Physico-chemical effects on the behaviour of a coastal mudslide. Geotechnique 46, 259–278.

Naudet, V., 2004. Les méthodes de résistivité électrique et de potentiel spontané appliquées aux sites contaminés (Thèse de geosciences de l'environnement). Université de droit, d'économie et des sciences-Aix-Marseille III, Marseille, France.

Naudet, V., Binley, A., 2006. A review of the self-potential method applied to groundwater investigations. Presented at the Proc. XVI International Conference on Computational Methods in Water Resources, Copenhagen, Denmark, pp. 18–22.

Naudet, V., Lazzari, M., Perrone, A., Loperte, A., Piscitelli, S., Lapenna, V., 2008. Integrated geophysical and geomorphological approach to investigate the snowmelt-triggered landslide of Bosco Piccolo village (Basilicata, southern Italy). Engineering Geology 98, 156–167.

Niesner, E., Weidinger, J., 2008. Investigation of a historic and recent landslide area in Ultrahelvetic sediments at the northern boundary of the Alps (Austria) by ERT measurements. The Leading Edge 27, 1498–1509.

Oliver, M.A., Webster, R., 1990. Kriging: a method of interpolation for geographical information systems. International journal of geographical information systems 4, 313–332. https://doi.org/10.1080/02693799008941549

Palis, E., Lebourg, T., Vidal, M., Levy, C., Tric, E., Hernandez, M., 2017. Multiyear time-lapse ERT to study short- and long-term landslide hydrological dynamics. Landslides 14, 1333–1343. https://doi.org/10.1007/s10346-016-0791-6

Panthulu, T.V., Krishnaiah, C., Shirke, J.M., 2001. Detection of seepage paths in earth dams using self-potential and electrical resistivity methods. Engineering Geology 59, 281–295. https://doi.org/10.1016/S0013-7952(00)00082-X

Patella, D., 1997. Introduction to ground surface self-potential tomography. Geophysical Prospecting 45, 653–681.

Pazzi, V., Morelli, S., Fanti, R., 2019. A Review of the Advantages and Limitations of Geophysical Investigations in Landslide Studies. International Journal of Geophysics 2019, 1–27. https://doi.org/10.1155/2019/2983087

Perrone, A., Iannuzzi, A., Lapenna, V., Lorenzo, P., Piscitelli, S., Rizzo, E., Sdao, F., 2004. High-resolution electrical imaging of the Varco d'Izzo earthflow (southern Italy). Journal of Applied Geophysics 56, 17–29.

Perrone, A., Lapenna, V., Piscitelli, S., 2014. Electrical resistivity tomography technique for landslide investigation: A review. Earth-Science Reviews 135, 65–82. https://doi.org/10.1016/j.earscirev.2014.04.002

Perry, J.W., Corry, C.E., Madden, T., 1996. Monitoring leakage from underground storage tanks using spontaneous polarization (SP) method, in: SEG Technical Program Expanded Abstracts 1996. Presented at the SEG Technical Program Expanded Abstracts 1996, Society of Exploration Geophysicists, pp. 932–935. https://doi.org/10.1190/1.1826811

Revil, A., Jardani, A., 2013. The Self-Potential Method: Theory and Applications in Environmental Geosciences. Cambridge University Press. https://doi.org/10.1017/CBO9781139094252

Revil, A., Naudet, V., Meunier, J.D., 2004. The hydroelectric problem of porous rocks: inversion of the position of the water table from self-potential data. Geophysical Journal International 159, 435–444. https://doi.org/10.1111/j.1365-246X.2004.02422.x

Revil, A., Pezard, P.A., Glover, P.W.J., 1999. Streaming potential in porous media: 1. Theory of the zeta potential. Journal of Geophysical Research: Solid Earth.

Robert, T.J.S., 2012. Geophysical identification, characterization, and monitoring of preferential groundwater flow paths in fractured media 183.

Roubinet, D., Linde, N., Jougnot, D., Irving, J., 2016. Streaming potential modeling in fractured rock: Insights into the identification of hydraulically active fractures. Geophysical Research Letters 43, 4937–4944.

Santoso, B., Hasanah, M.U., Setianto, 2019. Landslide investigation using self potential method and electrical resistivity tomography (Pasanggrahan, South Sumedang, Indonesia). IOP Conf. Ser.: Earth Environ. Sci. 311, 012068. https://doi.org/10.1088/1755-1315/311/1/012068

Sausse, J., 1998. Caractérisation et modélisation des écoulements fluides en milieu fissuré. Relation avec les altérations hydrothermales et quantification des paléocontraintes. (Thèse de géologie appliquée). Université Henri Poincaré - Nancy I, Nancy, France.

Schmutz, M., Guérin, R., Andrieux, P., Maquaire, O., 2009. Determination of the 3D structure of an earthflow by geophysical methods: the case of Super Sauze, in the French southern Alps. Journal of Applied Geophysics 68, 500–507.

Shevnin, V., Mousatov, A., Ryjov, A., Delgado-Rodriquez, O., 2007. Estimation of clay content in soil based on resistivity modelling and laboratory measurements. Geophys Prospect 55, 265–275. https://doi.org/10.1111/j.1365-2478.2007.00599.x

Siegel, D.I., Bickford, M.E., Orrell, S.E., 2000. The use of strontium and lead isotopes to identify sources of water beneath the Fresh Kills landfill, Staten Island, New York, USA. Applied Geochemistry 493–500.

Skianis, G.A., 2012. The Self-Potential Anomaly Produced by a Subsurface Flow at the Contact of Two Horizontal Layers and Its Quantitative Interpretation. International Journal of Geophysics 1–8.

Sudha, K., Israil, M., Mittal, S., Rai, J., 2009. Soil characterization using electrical resistivity tomography and geotechnical investigations. Journal of Applied Geophysics 67, 74–79. https://doi.org/10.1016/j.jappgeo.2008.09.012

Sujitapan, C., Kendall, M., Whiteley, J., Chambers, J., Uhlemann, S., 2019. Landslide Investigation and Monitoring Using Self-Potential Methods. Presented at the 25th European Meeting of Environmental and Engineering Geophysics, European Association of Geoscientists & Engineers, pp. 1–5.

Suski, B., Revil, A., Titov, K., Konosavsky, P., Voltz, M., Dagès, C., Huttel, O., 2006. Monitoring of an infiltration experiment using the self-potential method: self-potential monitoring of groundwater flow. Water Resour. Res. 42. https://doi.org/10.1029/2005WR004840

Tavenas, F., Leroueil, S., 1981. Creep and failure of slopes in clays. Canadian Geotechnical Journal 18, 106–120.

Telford, W.M., Sheriff, R.E., 1990. Applied geophysics. Cambridge university press.

Titov, K., Ilyin, Yu., Konosavski, P., Levitski, A., 2002. Electrokinetic spontaneous polarization in porous media: petrophysics and numerical modelling. Journal of Hydrology 267, 207–216. https://doi.org/10.1016/S0022-1694(02)00151-8

Travelletti, J., Malet, J.-P., 2012. Characterization of the 3D geometry of flow-like landslides: A methodology based on the integration of heterogeneous multi-source data. Engineering Geology 128, 30–48. https://doi.org/10.1016/j.enggeo.2011.05.003

Van Den Eeckhaut, M., Verstraeten, G., Poesen, J., 2007. Morphology and internal structure of a dormant landslide in a hilly area: The Collinabos landslide (Belgium). Geomorphology 89, 258–273. https://doi.org/10.1016/j.geomorph.2006.12.005

Varnes, D.J., 1978. Slope movement types and processes. Special report, National Academy of Sciences 176, 11–33.

Whiteley, J.S., Chambers, J.E., Uhlemann, S., Wilkinson, P.B., Kendall, J.M., 2019. Geophysical Monitoring of Moisture-Induced Landslides: A Review. Rev. Geophys. 57, 106–145. https://doi.org/10.1029/2018RG000603